# Mesoscale Model Simulations of Three Heavy Precipitation Events in the Western Mediterranean Region

ROMUALDO ROMERO, CLEMENTE RAMIS, AND SERGIO ALONSO

*Meteorology Group, Department of Physics, University of the Balearic Islands, Palma de Mallorca, Spain*

CHARLES A. DOSWELL III AND DAVID J. STENSRUD

*NOAA/ERL National Severe Storms Laboratory, Norman, Oklahoma*

(Manuscript received 18 January 1997, in final form 20 October 1997)

ABSTRACT

A mesoscale numerical model with parameterized moist convection is applied to three cases involving heavy rainfall in the western Mediterranean region. Forecast precipitation fields, although not perfect when compared to the observations of rainfall, appear to have sufficient information to be considered useful forecasting guidance. The results illustrate that a good simulation for this type of event in a region with complex topography is strongly dependent on a good initialization and prediction of the low-level flow and water vapor distribution.

For two of the cases that have a marked synoptic-scale contribution, the simulations give reasonably accurate predictions of the precipitation distribution, although the amounts are generally underestimated. The third case exhibits relatively subtle synoptic-scale forcing and is dominated by isolated convective storms (mostly over the sea) that also produced severe thunderstorms (including tornadoes), and the prediction of precipitation is not as promising. Overall, the results are encouraging in terms of potential application of mesoscale models operationally in the western Mediterranean region. Additional experiments beyond the ''control'' simulations have been performed to isolate the influence of orography and water vapor flux from the Mediterranean Sea on the model simulations. This factor separation indicates that both effects can be important contributors to a successful forecast. Suggestions are offered for future efforts in pursuing the application of mesoscale models to this forecast problem.

## 1. Introduction

Heavy precipitation is a serious weather hazard in the western Mediterranean region (Fig. 1), as discussed by, among others, García-Dana et al. (1982), Ramis et al. (1986), Llasat (1987), and Ramis et al. (1994). It is mostly the result of deep, moist convection, which can lead to significant amounts of precipitation in a short time. Extraordinary observations of such heavy precipitation include a case of more than 200 mm of rainfall in 2 h in Ibiza (in the Balearic Islands) on 15 November 1985 (described in Ramis et al. 1986), and a situation with more than 800 mm of rainfall in 24 h in Gandía (within Valencia, in mainland Spain) on 3 November 1987 (Fernández et al. 1995).

Significant reduction of the hazards to human life associated with heavy precipitation is possible if the heavy rainfall occurrence can be forecast reliably, although the short timescales often mean that property losses from flash floods are difficult to mitigate. We are concerned, therefore, with how to improve the capabilities of the operational forecasting agencies within the region to anticipate properly these potentially devastating events.

For the purposes of this study, the western Mediterranean region is defined to be the western part of the Mediterranean Sea and surrounding lands, comprising the eastern Spanish mainland, southern France, Corsica, Sardinia, and northern Africa (Meteorological Office 1954). In a companion paper (Doswell et al. 1998; hereafter DRRA98), we have described and analyzed the observed synoptic evolution of three events (referred to as the ''Algeria,'' ''Piedmont,'' and ''Menorca'' cases in DRRA98) that produced heavy rainfall in the western Mediterranean region. This paper addresses the mesoscale numerical model simulations of the same three cases, with a special emphasis on the spatial distribution of the rainfall produced by the simulations. Also, in addition to the ''control'' simulations, some additional experiments were conducted to isolate the impacts of orography and sea surface water vapor fluxes, using the factor separation concept introduced by Stein and Alpert (1993).

Although the cases are described extensively in DRRA98, we include short summaries here to make this

*Corresponding author address:* Dr. Charles A. Doswell III, National Severe Storms Laboratory, 1313 Halley Circle, Norman, OK 73069.
E-mail: doswell@nssl.noaa.gov

© 1998 American Meteorological Society

Unauthenticated | Downloaded 08/02/21 05:51 AM UTC

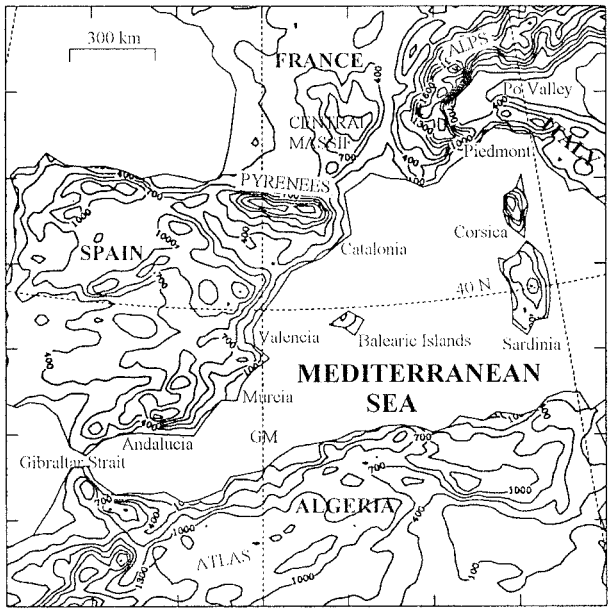


FIG. 1. The western Mediterranean region with its orography (contour interval is 300 m starting at 100 m). The sites mentioned in the text are indicated.

paper self-contained. The first, called the ''Algeria'' event, was characterized by a stagnant synoptic pattern (Fig. 2) during the period 31 January–7 February 1993. As a result, strong low-level winds advected moisture toward the eastern coast of Spain. Moderate to heavy daily rainfall occurred in eastern Spain (especially in Valencia; see Fig. 1) from 1 to 7 February, except on 5 February. Although the exact amounts and locations of the rainfall varied from day to day, the pattern of rainfall each day was similar to that shown in Fig. 3, from 2 February.

The second case, the ''Piedmont'' event, refers to the heavy rains that occurred in northwestern Italy during the period 4–6 November 1994. Whereas the pattern in the Algeria case was stagnant, this case was characterized by a strong, mobile trough (Fig. 4) with a marked cold front crossing the western Mediterranean area. Ahead of the advancing front, strong low-level winds brought moisture northward and impinged on the complex terrain of northwestern Italy and nearby parts of France. Rainfall totals exceeded 200 mm over a wide region on 5 November (Fig. 5) and, as discussed in DRRA98, nonconvective precipitation plays an important role.

The third case, called the ''Menorca'' event, occurred on 8 October 1992. At the synoptic scale, the event appears to be associated with a short-wave trough embedded in a larger cyclone just to the southwest of the Iberian Peninsula (Fig. 6). Two mesoscale convective systems developed over the western Mediterranean Sea producing heavy rainfall in Valencia on mainland Spain (Fig. 7) and a tornado on Menorca in the Balearic Islands. During the heavy precipitation in Valencia, the moist easterly flow at low levels from over the Mediterranean encountered the complex coastal terrain of the area.

In DRRA98, it was shown that some superficial synoptic-scale similarities exist among these three events. That is, on the day of the event, all of the cases had a strong synoptic-scale trough or closed cyclone at upper levels, west of the threat area. Along with this common structure aloft, moist air is being advected upslope in each case at low levels. These common features might be interpreted to suggest that forecasting heavy rainfalls in the western Mediterranean region ought to be easy. However, the details of when and where the heavy rain is expected within the broad synoptic pattern, as well as the intensity of the rainfall, appear to be challenging problems for operational synoptic-scale numerical prediction models.

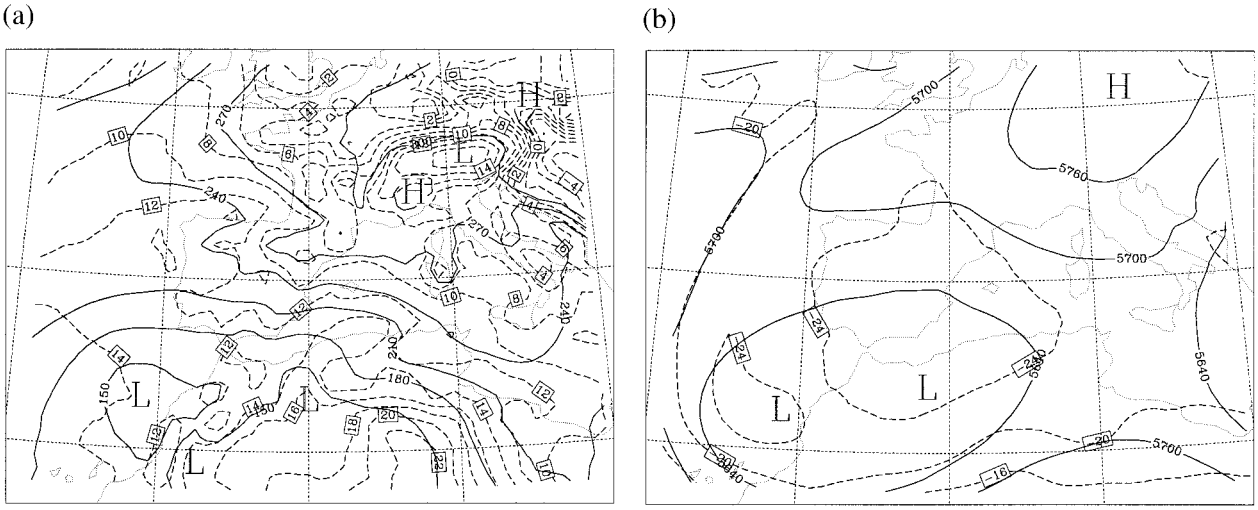


FIG. 2. Meteorological situation on 2 February 1993 at 0000 UTC from ECMWF data: (a) 1000 and (b) 500 hPa. Isohypses (solid line) and isotherms (dashed) are shown.

Unauthenticated | Downloaded 08/02/21 05:51 AM UTC

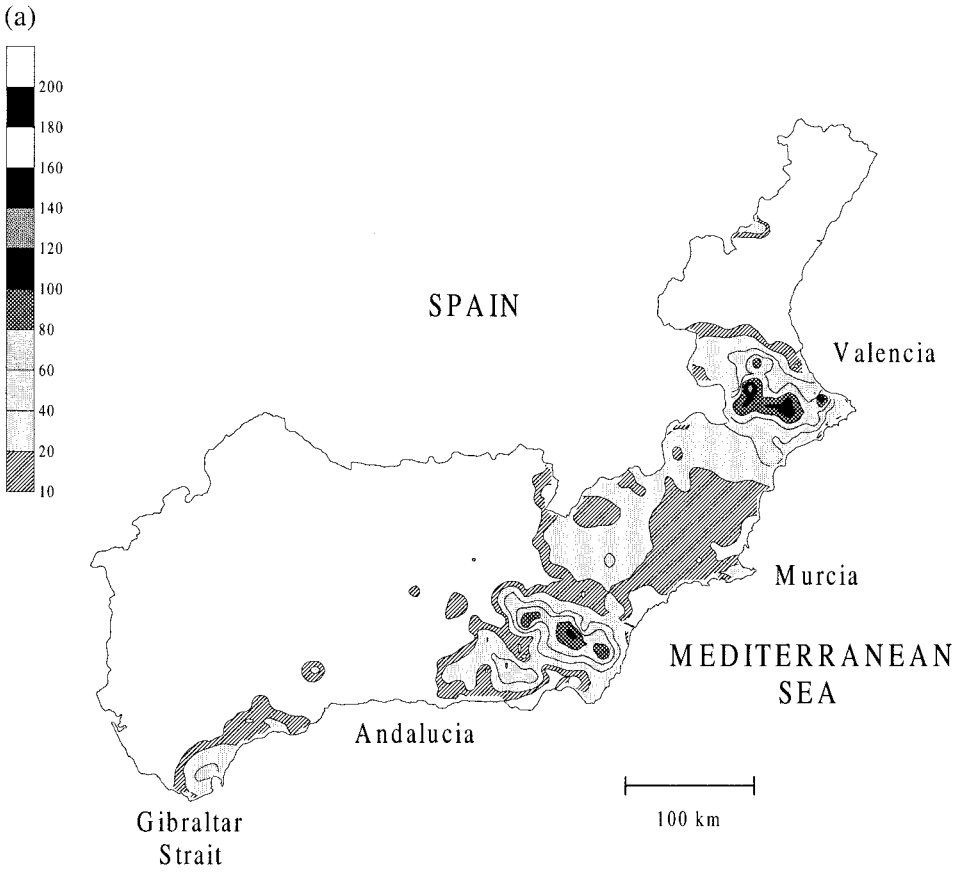


FIG. 3. Observed precipitation (mm; see the key) in eastern and southern Spain from 0700 UTC 2 February to 0700 UTC 3 February 1993. (b) The location of the area analyzed.

Forecast users generally are interested in what is happening in their immediate vicinity, not something occurring 150 km away. From one viewpoint, a forecast of heavy rainfall over the eastern coast of mainland Spain on a given day would be an excellent forecast if 200 mm rainfall is observed in Andalusia. However, if the citizens of Catalonia or Valencia experience clear skies all day at the same time, they might be unhappy with such a forecast. A logical question to ask, therefore, is whether or not a mesoscale simulation model would offer useful additional information for operational forecasters. Can such a model produce valuable guidance often enough to justify an operational implementation? Can such a model produce enough quantitative improvement, in terms of time and space specificity of the quantitative precipitation forecasts (QPF), over the present operational forecast models, to justify the investment in operational mesoscale models?

Although some previous numerical simulations of heavy rainfall events in the western Mediterranean region exist (e.g., Paccanella et al. 1992; Fernández et al. 1995; Romero et al. 1997), this study marks a new effort

Unauthenticated | Downloaded 08/02/21 05:51 AM UTC

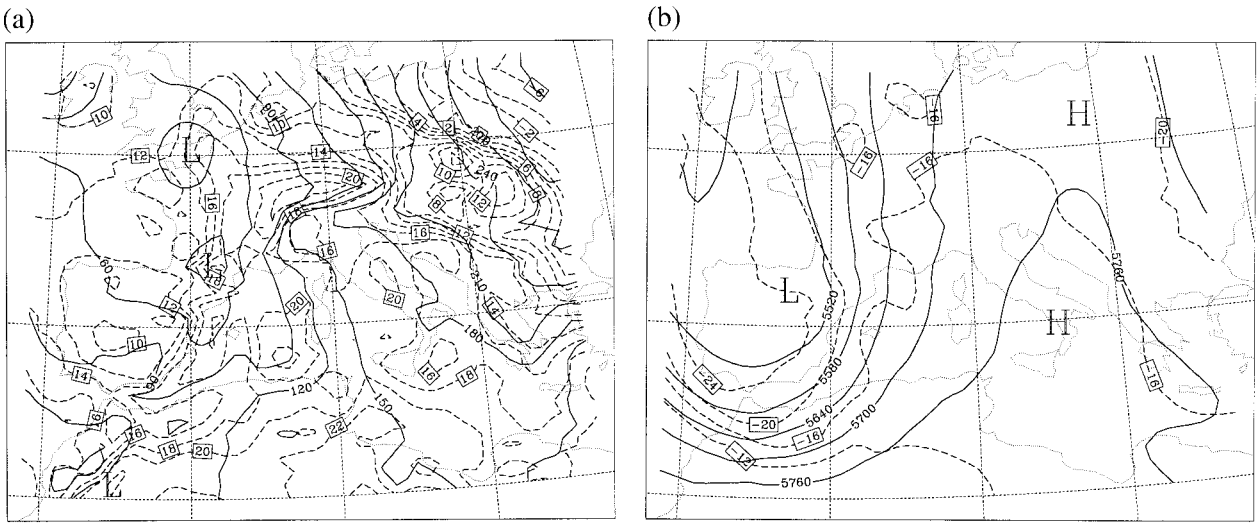


FIG. 4. As in Fig. 2 except at 0000 UTC 5 November 1994.

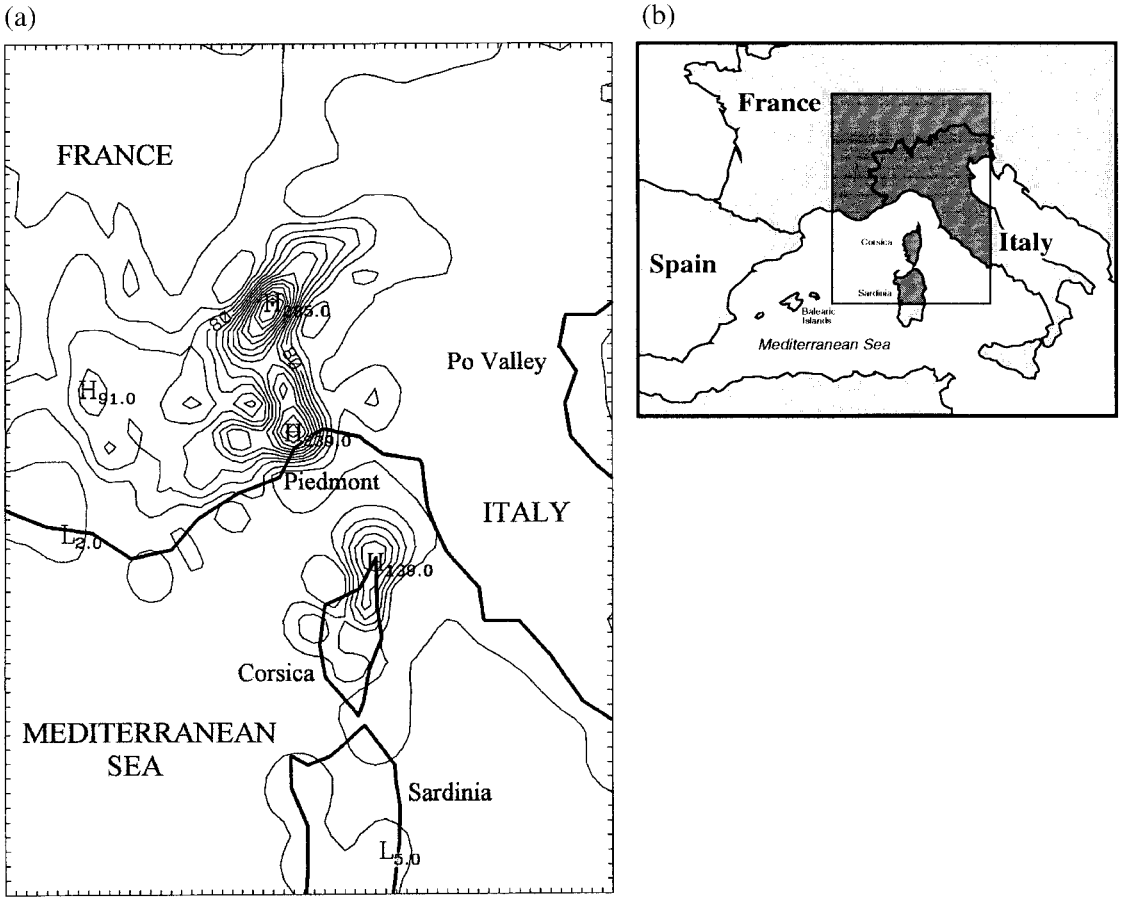


FIG. 5. Observed precipitation (mm) in the Piedmont vicinity (see Fig. 1), from 0000 to 2400 UTC 5 November 1994. Note that contours over the ocean are the result of an objective analysis rather than the existence of precipitation measurements over the sea. (b) The location of the area analyzed.

Unauthenticated | Downloaded 08/02/21 05:51 AM UTC

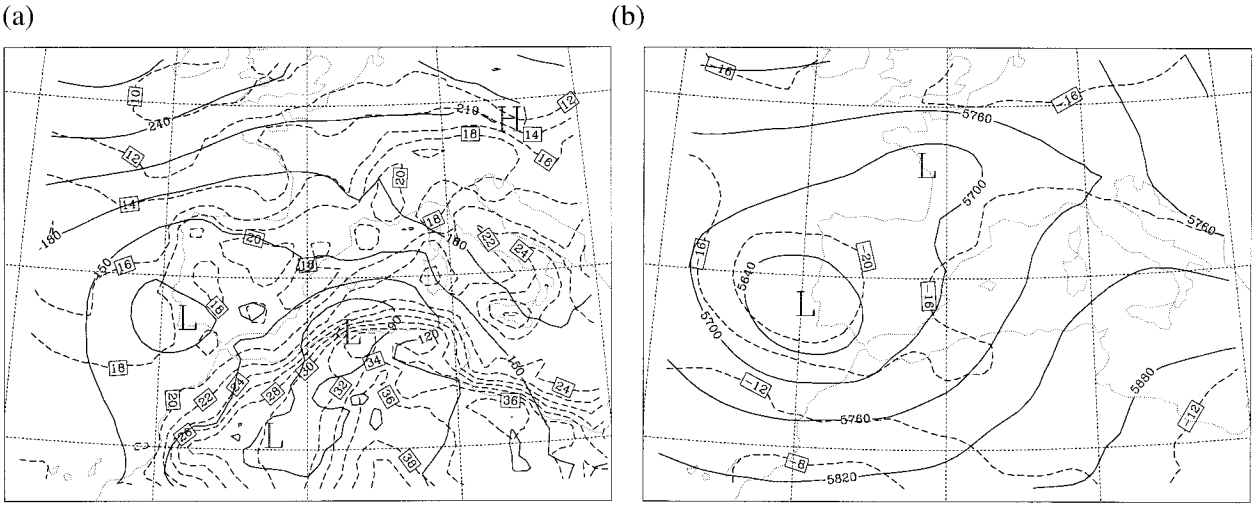


FIG. 6. As in Fig. 2 except at 1200 UTC 8 October 1992.

to address the feasibility of operational mesoscale modeling, notably in the western Mediterranean region. As such, this work cannot provide a definitive answer to the questions we have posed. Rather, it is an effort to see if additional resources should be invested to obtain a more definitive answer than that which can be provided from a limited number of cases. Although the model used has been described extensively elsewhere (Romero et al. 1997), we provide a short summary of its main aspects in section 2. Section 3 will focus on the details of how the numerical simulations were carried out for our three cases. Section 4 then provides results of the simulations, and section 5 considers quantitatively the impacts of orography and sea surface water vapor fluxes on the simulations. Section 6 then presents an interpretation of the model results in terms of what they indicate about the simulations as operational forecast guidance.

## 2. Model description

The simulations were performed using the hydrostatic three-dimensional, mesoscale model developed originally by Nickerson et al. (1986). This model has shown its ability to simulate a wide range of mesoscale flows. For example, the model has been used to simulate mesoscale airflow induced by vegetation or soil moisture inhomogeneities (Mahfouf et al. 1987a; Pinty et al. 1989), downslope windstorms (Richard et al. 1989), mountain waves (Nickerson et al. 1986; Romero et al. 1995), and the sea-breeze circulation [in Florida by Mahfouf et al. (1987b); in Mallorca by Ramis and Romero (1995)]. Recently, it also has been used to simulate a heavy rainfall event in the western Mediterranean that affected the region of Catalonia (Romero et al. 1997). The numerical model is appropriate for complex-terrain simulations like the western Mediterranean region since it uses a terrain-following vertical coordinate, with high resolution in the planetary boundary layer [PBL; Nickerson et al. (1986)].

Resolvable-scale rain is predicted in the model following the warm microphysical parameterization described in Nickerson et al. (1986). The governing equations for water substance include one for water vapor plus cloud water mixing ratio, and two for the rainwater mixing ratio and the number concentration of raindrops. These include Kessler-type autoconversion, self-collection, accretion, evaporation, and sedimentation source–sink processes, based on an assumed lognormal raindrop distribution.

Horizontal diffusion is introduced explicitly by a second-order operator. The vertical turbulent mixing is expressed through an eddy-diffusivity assumption with a 3/2-order closure: the exchange coefficients are calculated as functions of the turbulent kinetic energy (predicted by the model) and the mixing length scale, following Therry and Lacarrère (1983) and Bougeault and Lacarrère (1989).

At the surface, turbulent fluxes of momentum, heat, and moisture are calculated following Louis (1979). In order to account for diurnal effects, a two-layer, force–restore method for the ground temperature (Bhumralkar 1975; Blackadar 1976) has been implemented. The surface properties (albedo, emissivity, roughness, thermal inertia, and available moisture) all are specified with a single surface index under the assumption that these properties appear related for natural surfaces (Benjamin and Carlson 1984). A realistic spatial distribution of the soil index allows us to represent the effect of surface heterogeneities on atmospheric circulations (Benjamin and Carlson 1984). This method is simple but does not represent the effects of rainfall episodes on the surface energy budget components at subsequent simulation times. Rather, the surface parameters and, more critically, the available moisture for evaporation, are kept

Unauthenticated | Downloaded 08/02/21 05:51 AM UTC

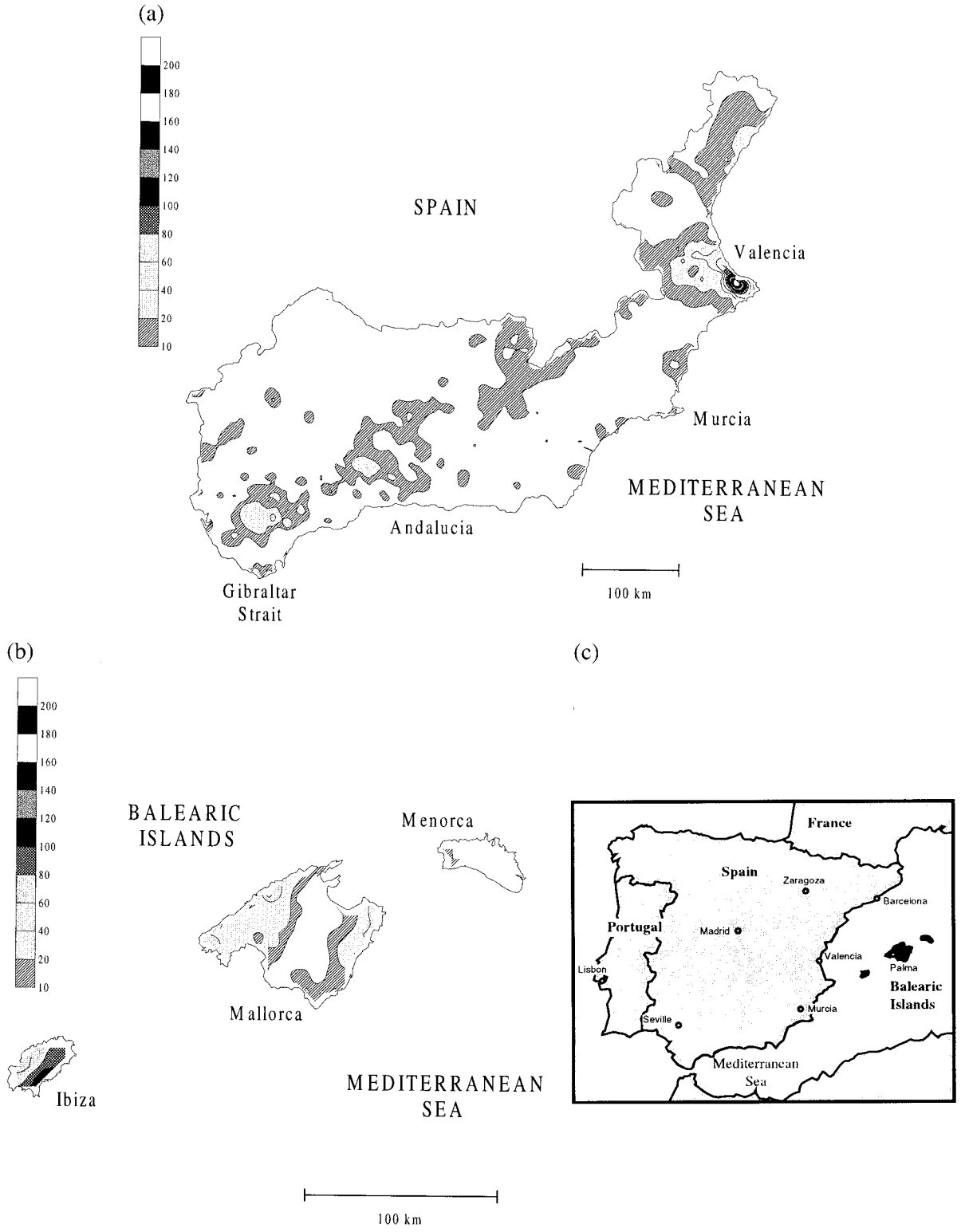


FIG. 7. Observed precipitation (mm; see the key) from 0700 UTC 8 October to 0700 UTC 9 October 1992. (a) In eastern and southern Spain (see inset in Fig. 3 for location); (b) in the Balearic Islands [(c) shows the location of the area analyzed].

Unauthenticated | Downloaded 08/02/21 05:51 AM UTC

constant during the simulation. Given the lack of a database of surface parameters to be specified in order to run more complete surface physics packages, and since we are not dealing with long-range simulations, this method seems reasonable.

Solar and infrared fluxes across the atmosphere, which determine the net radiation at the surface and contribute to the diabatic term of the thermodynamic equation by the flux divergence, are based on the method given by Mahrer and Pielke (1977). Scattering and absorption of solar radiation by permanent gases such as oxygen, ozone, and carbon dioxide are included. Absorption and longwave emission by the atmospheric water constituents (water vapor and clouds) are also considered. The surface radiative fluxes are modified to account for the terrain slope, as well.

### *a. Cumulus convective parameterization*

As in Romero et al. (1997), the cumulus convection scheme of Emanuel (1991) has been used. The scheme is based on the dynamics and microphysics of convection as revealed by observations (notably, aircraft). The fundamental entities for moist convective transport are the subcloud-scale drafts rather than the clouds. Unlike some other schemes based on bulk-entraining plumes (e.g., Fritsch and Chappell 1980; Arakawa and Schubert 1974), convective transports are idealized based on reversible ascent of the subcloud-scale entities, mixing, and buoyancy sorting (Raymond and Blyth 1986). In the scheme, the updraft mass fluxes are functions of convective available potential energy (CAPE) so as to drive the mass fluxes toward a state of quasi-equilibrium with the large-scale (explicitly resolved) forcing.

### *b. Initialization and boundary conditions*

The orographic database (U.S. Navy) and large-scale meteorological fields in the form of uninitialized analyses on standard pressure surfaces from the European Centre for Medium-Range Weather Forecasts (ECMWF) are given on regular latitude–longitude grids, with intervals of 5′ for the orography and 0.75° for the ECMWF analyses. These data are interpolated to our regular $x$–$y$ model grid coordinates, which use a polar stereographic projection. Orographic data are interpolated linearly to the model grid points. In order to avoid excessive forcing by the smallest resolvable scales, the interpolated orography is smoothed with a two-step filter (Shapiro 1970).

The synoptic-scale meteorological fields provided are temperature, relative humidity, geopotential height, and the two components of the horizontal wind. For the temperature and humidity, the fields are mapped onto the model grid (on the $p$ surfaces) with a successive corrections univariate method (Pedder 1993). With an appropriate scale parameter for the Gaussian-weighted scheme, the method smooths the original data while retaining the meso-$\alpha$-scale structures.

For the wind and geopotential fields, a mass–wind balance is imposed whereby the geopotential adjusts to the ''observed'' winds. This process is done in two steps. During the first step, the streamfunction and wind (including a divergent component) are analyzed on each isobaric surface with the statistical technique described by Pedder (1989) on the wind data. This avoids the empirical specification of external boundary conditions on streamfunction and velocity potential needed in methods that solve for the wind from estimated values of vorticity and divergence. In the second step, as in Warner et al. (1978), the geopotential $\phi$ is calculated from the streamfunction $\psi$ by solving the balance equation

$$\nabla^2\phi = f(\psi_{xx} + \psi_{yy}) - 2m^2(\psi_{xy}^2 - \psi_{xx}\psi_{yy}) + f_y\psi_y + f_x\psi_x,$$

where $m$ is the map factor, $f$ the Coriolis parameter, and subscripts denote partial derivatives. Boundary values for $\phi$ are given by direct analysis of the geopotential heights. Sea level data are extrapolated from 1000 hPa assuming a standard atmosphere temperature lapse rate and constant relative humidity.

The pressure is determined hydrostatically and the wind is set to zero. Once the analyzed fields are interpolated to the vertical levels of the mesoscale model, the vertical profiles of geopotential and temperature are slightly modified at each grid point to force the hydrostatic adjustment. This is done via a variational method to minimize the corrections to both fields throughout the depth of the column.

The wind, which is interpolated linearly with the already-corrected values of the geopotential height to preserve the mass–wind balance, is also slightly modified after applying a variational adjustment that minimizes the vertical integral of the horizontal divergence (Pinty 1984). The aim of this dynamic adjustment is to filter gravity waves.

This initialization is probably superfluous when we are using dense and uniformly distributed ''observed'' data, as in the ECMWF analyses. In fact, some experiments (not shown) initialized with simple linear interpolation, and not doing the hydrostatic and dynamic adjustments, showed that although the simulations are not as smooth, the output fields and, more specifically, the precipitation fields, are basically unchanged except for minor details. Nevertheless, we have retained this procedure in our simulations.

At the top of the model, the vertical velocity in the terrain-following coordinate is set to zero. To minimize reflection from the upper boundary, an absorbing layer is included, with the background diffusion increasing progressively with height to a maximum at the topmost level.

One-way nesting of the mesoscale model allows assimilation of the external forcing, which is given by time-dependent lateral boundary conditions. At any given time, the fields at the boundaries are determined by linear in-

Unauthenticated | Downloaded 08/02/21 05:51 AM UTC

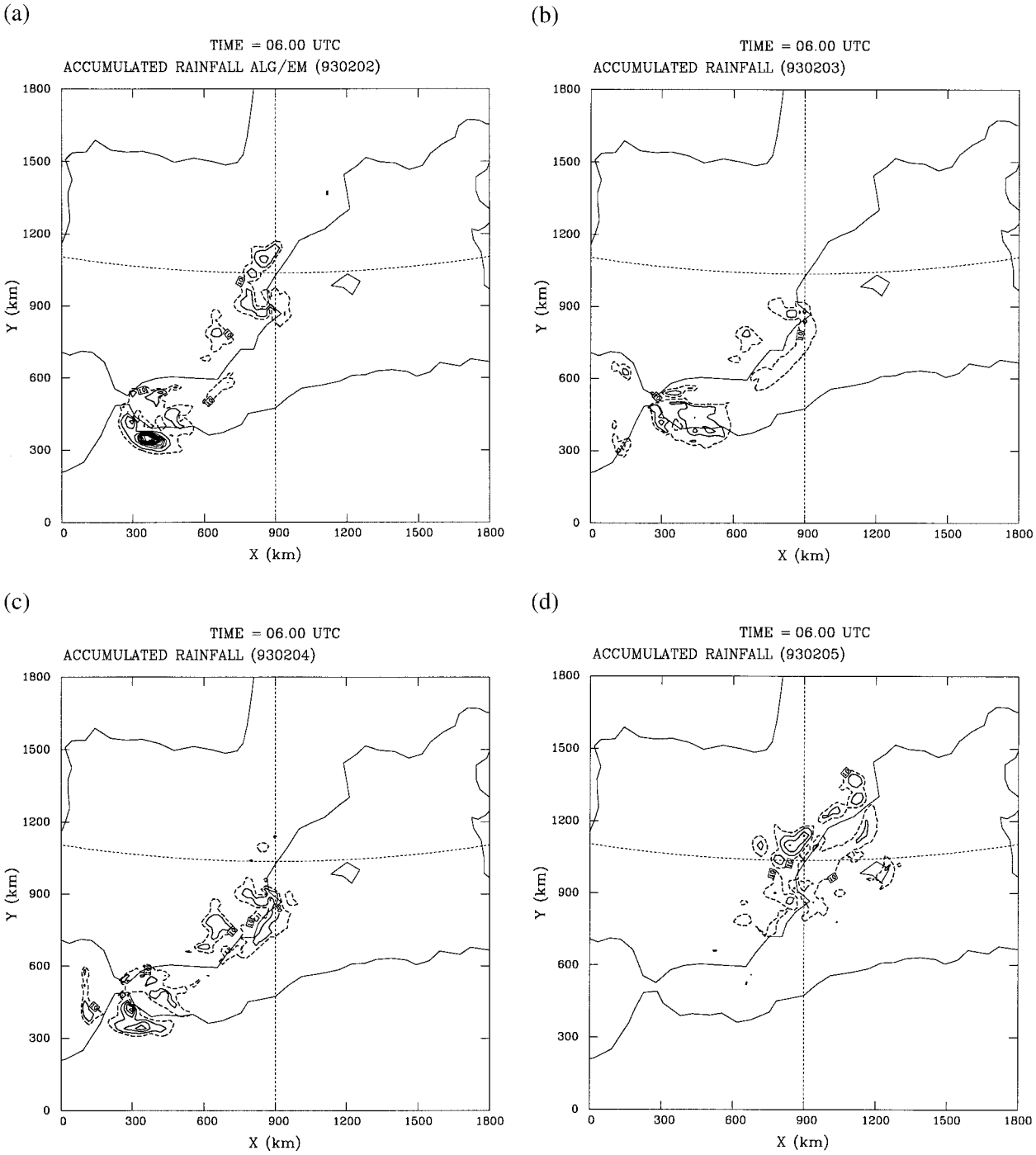


FIG. 8. Model forecast precipitation for the Algeria case, accumulated from 0600 UTC to 0600 UTC (next day): (a) on 1 February, (b) on 2 February, (c) on 3 February, (d) on 4 February 1993. Contour interval is 20 mm, starting at 20 mm (solid line); dashed contour corresponds to 10 mm.

→

FIG. 9. Observed precipitation (mm; see the key) in eastern and southern Spain from 0700 UTC to 0700 UTC (next day): (a) on 1 February, (b) on 3 February, (c) on 4 February 1993 (in Catalonia and Valencia). For (a) and (b), the location is shown in the inset for Fig. 3; the location of area (c) is shown in (d).

Unauthenticated | Downloaded 08/02/21 05:51 AM UTC

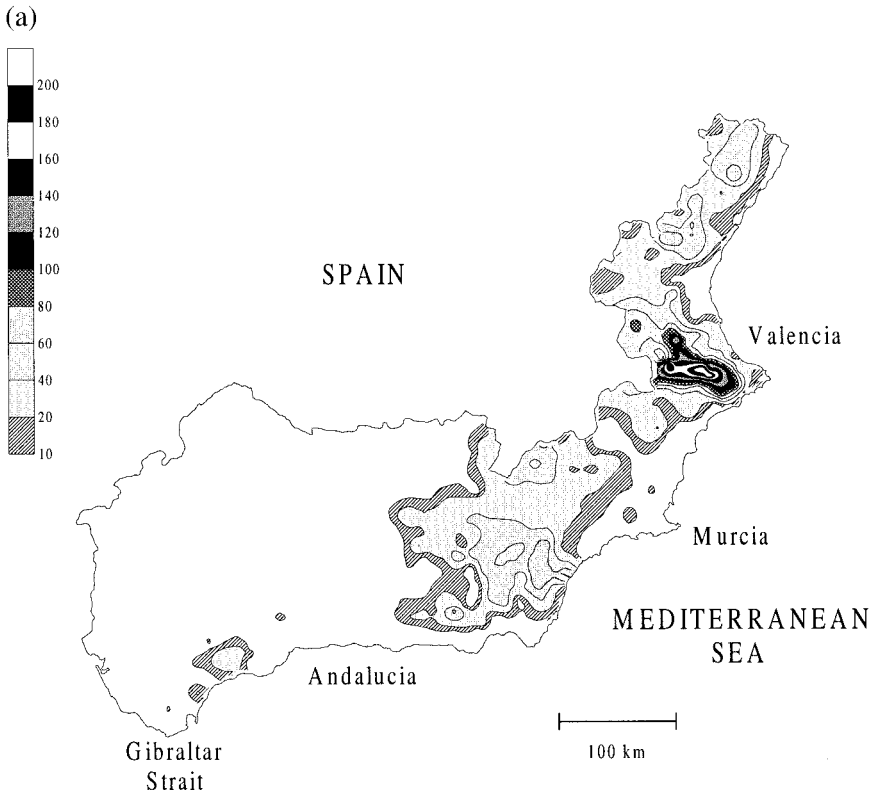


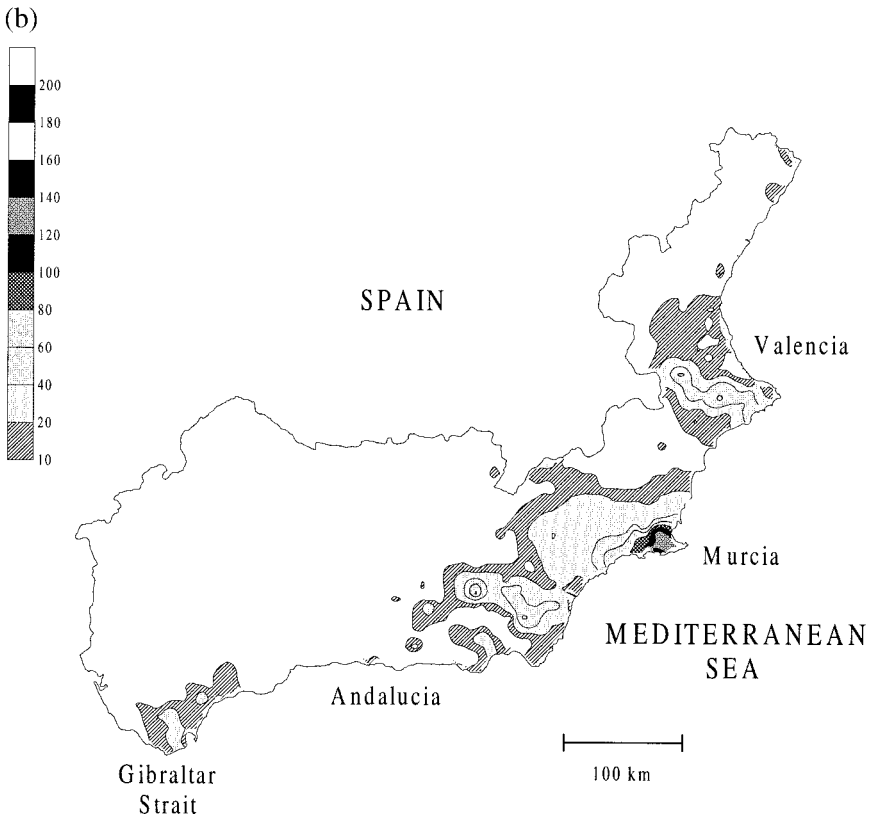


Unauthenticated | Downloaded 08/02/21 05:51 AM UTC

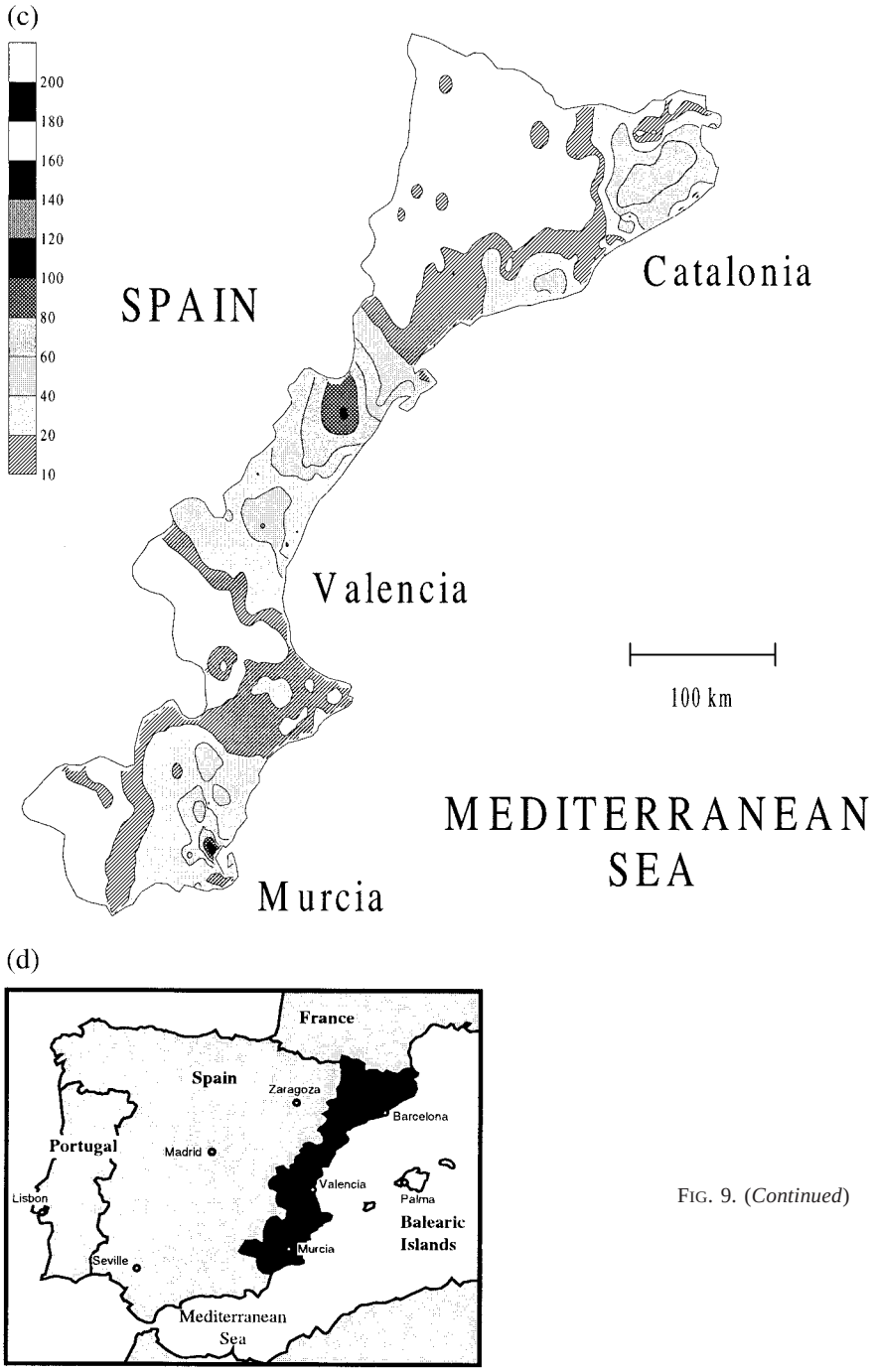


FIG. 9. (*Continued*)

terpolation between the values at the available ECMWF analysis times (every 6 h). The method of Davies (1976) is applied to minimize reflections while relaxing the interior values of the fields to the boundary values.

## 3. The case studies

We have already noted the superficial similarities among our three cases. These similarities suggest that, with similar synoptic patterns and the complex topography of the western Mediterranean region, a mesoscale model is likely to be at least moderately successful. That is, if heavy rainfalls in the region have a large synoptic-scale component that is modulated by the complex topography, then we have hypothesized that a mesoscale model should do well. If, on the other hand, for successful simulations there are important mesoscale details that must be specified accurately in

Unauthenticated | Downloaded 08/02/21 05:51 AM UTC

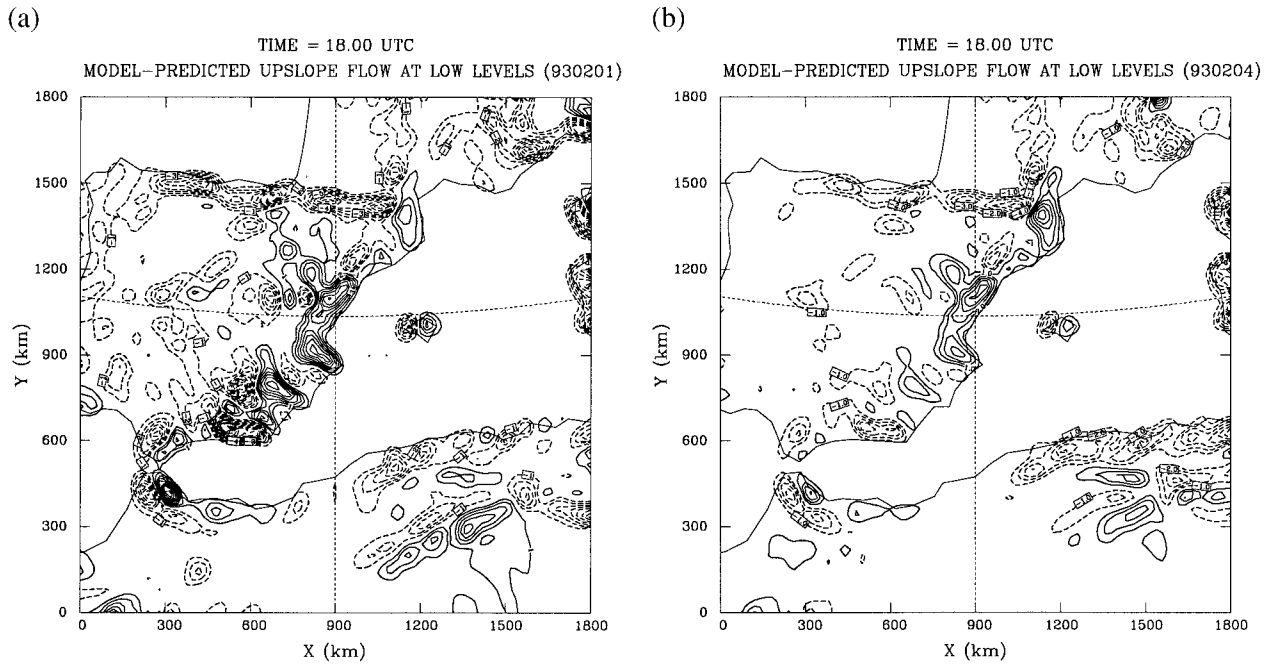


FIG. 10. Model predicted upslope flow (using winds at 4.5 m AGL, the lowest model level) for the Algeria case: (a) at 1800 UTC 1 February 1993 (simulation starting at 0000 UTC), (b) at 1800 UTC 4 February 1993 (starting at 0000 UTC). Contour interval is 1 cm $s^{-1}$, starting at 1 cm $s^{-1}$; solid lines indicate upward motion.

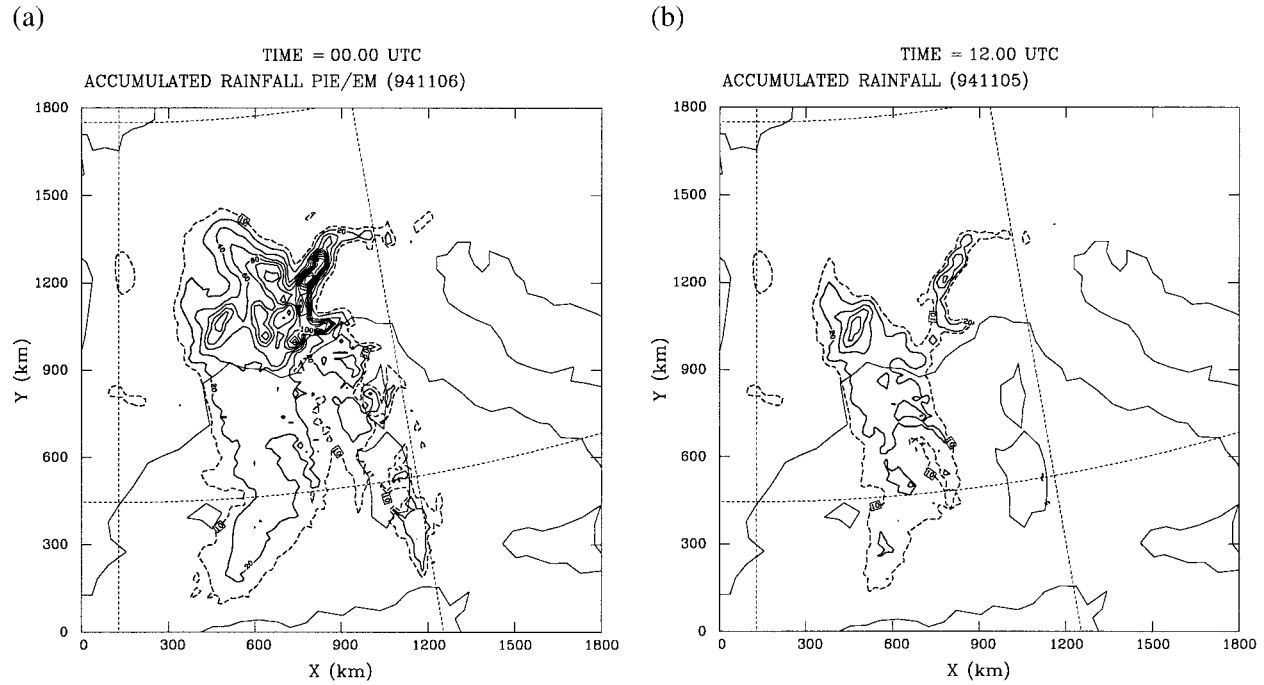


FIG. 11. Model forecast precipitation for the Piedmont case: (a) accumulated from 0000 to 2400 UTC 5 November, (b) accumulated from 0000 to 1200 UTC 5 November 1994. Contour interval is 20 mm starting at 20 mm (solid line); dashed contour corresponds to 10 mm.

Unauthenticated | Downloaded 08/02/21 05:51 AM UTC

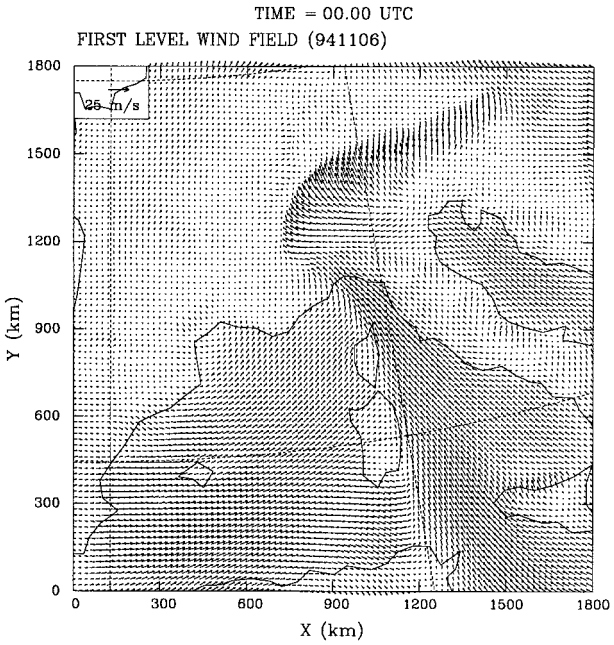


FIG. 12. Model forecast surface wind field (using winds at 4.5 m AGL) for the Piedmont case at 0000 UTC 6 November 1994 (simulation starting at 1800 UTC 4 November). The arrow on the upper left corner represents 25 m $s^{-1}$.

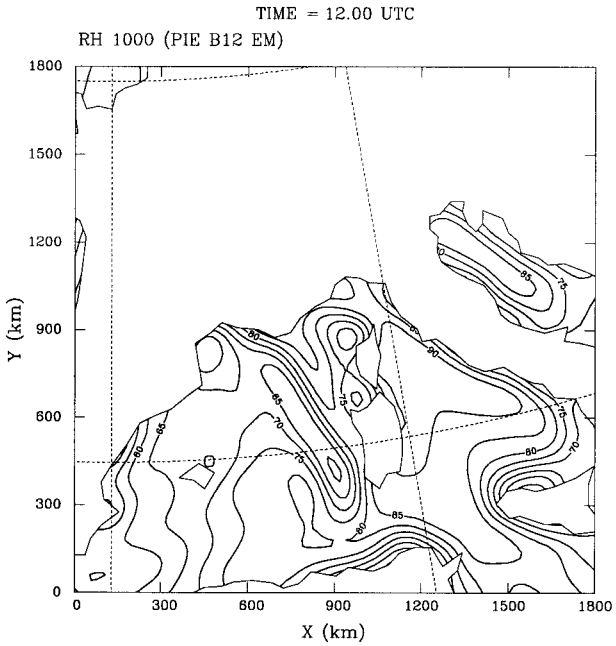


FIG. 13. The 1000-hPa relative humidity (contour interval of 5%) from the model simulation at 1200 UTC 5 November 1994.

the initial conditions, such cases are less likely to be well simulated (Stensrud and Fritsch 1994). The numerical experiments described herein are designed, in part, to address this hypothesis.

The Algeria, Piedmont, and Menorca numerical experiments followed the procedures described in section 2. The grid size was fixed for the three cases, with a nominal horizontal grid length of 20 km and 30 vertical levels (the lowest level being 4.5 m AGL). The 91 × 91 horizontal grid, therefore, covered a square domain 1800 km on a side, but the computational domain was centered according to the geographical region affected by the heavy precipitation in each case (grid center at 39°N, 0° for the Algeria and Menorca cases; 43°N, 8°E for Piedmont). This minimizes the effect of lateral boundaries in the area of greatest interest.

The surface submodel requires the soil type distribution to be specified. Based on NOAA AVHRR mosaics and other information, and following the classification given by Benjamin and Carlson (1985), a spatial distribution of seven land types has been derived for the western Mediterranean region. Owing to the season when the events occurred, the values listed in Benjamin and Carlson (1984) for the available soil moisture have been increased by 0.2, 0.1, and 0.05 (where 1.0 corresponds to saturated soil and 0.0 to completely dry soil) for the Algeria, Piedmont, and Menorca cases, respectively. Sea surface temperatures for the three cases are provided by the ECMWF surface data, and subsoil temperatures correspond to the climatological values for February, November, and October, respectively.

For the Algeria case, we did a series of 30-h simulations from 0000 to 0600 UTC (the following day), for the period 1–4 February. The available Spanish rainfall observations used for verifying the precipitation predictions give 24-h rainfall totals from 0700 UTC to the following day at 0700 UTC. Starting the model at 0000 UTC corresponds to the standard synoptic rawinsonde

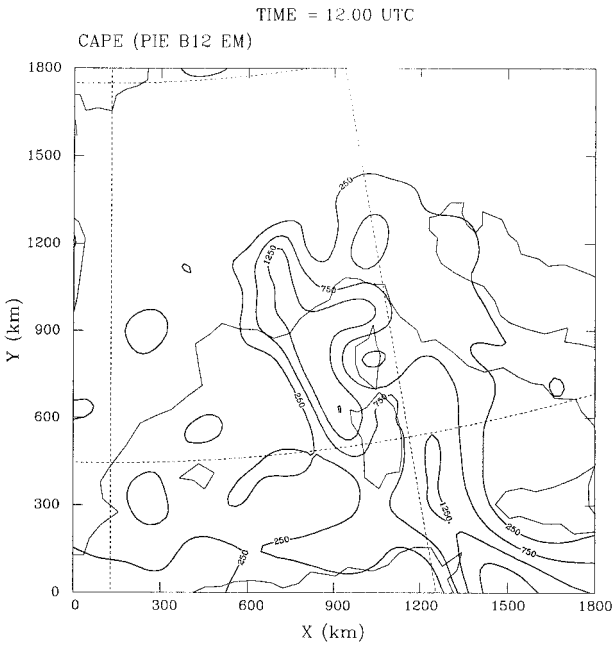


FIG. 14. As in Fig. 13 except for CAPE (contour interval is 500 J $kg^{-1}$, starting at 250 J $kg^{-1}$).

Unauthenticated | Downloaded 08/02/21 05:51 AM UTC

times and gives the model some ''spinup'' time before we evaluate the forecast precipitation.

Precipitation fell primarily on 8 October 1992 for the Menorca case, so only a single simulation was performed for that case. In the Piedmont case, the heaviest precipitation fell on 5 November 1994; the single simulation runs from 1800 UTC 4 November to 0000 UTC 6 November, since the precipitation data from the French and Italian 24-h rainfall observations is collected during the 0000–2400 UTC time interval.

## 4. Case study results

### *a. Algeria*

As noted in DRRA98, this episode occurs in the winter rather than the climatologically favored fall. The synoptic charts on any given day, however, could be quite misleading because (except for the temperature and dewpoint values) the pattern is not unlike a common fall structure for heavy precipitation. The associated tropospheric trough is very slow moving, and the ECMWF model forecasts were able to predict the slow large-scale movement successfully. This is a relevant issue for our mesoscale model simulation, since its time-dependent lateral boundary conditions come from the ECMWF model results.

The mesoscale model-predicted precipitation pattern for the first three days (Figs. 8a–c) is very similar, with substantial precipitation centers in the Valencia region and southeastern Spain. This changes on 4 February, when the important precipitation also begins to affect Catalonia in northeastern Spain and has practically ceased in southern Spain. This evolution of the simulated precipitation pattern is in agreement with the observed rainfall (Figs. 3 and 9), except that the simulation fails to reproduce the coastal maximum observed in eastern Andalucia. The model-predicted amounts are underestimates of the very localized peak observed values, but they do capture the patterns reasonably well.

The important role played by the coastal topography seems clear, as we shall demonstrate in the next section. The precipitation band is more or less parallel to the coastline and the maxima are strongly associated with important orographic features (cf. Figs. 1 and 8). High rainfall amounts are predicted by the model in northern Africa, near the Gibraltar Strait, in a region of significant terrain elevation. No data are available, unfortunately, to validate that aspect of the forecast.

Surface flow for the period (not shown) changes only slightly from day to day during the series of simulations, except on 4 February when it weakens appreciably in the south part of the western Mediterranean region and intensifies near Catalonia. Apart from upslope flow, there does not appear to be any mesoscale structure present that would localize the rainfall. The upslope flow, very moist as a result of a long fetch over the Mediterranean Sea, impinges on the coastal orography. By calculating the upslope flow component of the forecast surface winds, $\mathbf{V}_s \cdot \nabla h$, where $\mathbf{V}_s$ is the surface wind vector and $h$ is the terrain height, we can validate the importance of the upslope flow. As shown in Fig. 10a, the model forecasts considerable upslope flow in Valencia and the southeastern part of Spain during the first stages of the event (compare with Figs. 8a–c). Also encouraging is that the upslope flow predicted by the model for 4 February (Fig. 10b) shows that upslope flow weakening in southern Spain and strengthening in Catalonia, in good agreement with the observed shift in the heavy rainfall.

### *b. Piedmont*

The observed precipitation for this case (cf. Fig. 5) has a tongue of significant rainfall (up to 250 mm in 24 h) extending from the Mediterranean Sea coast roughly toward the north in the Piedmont region of northwestern Italy. As Fig. 11a shows, the model has simulated both the pattern and the amounts quite well, although the model has overpredicted the rainfall in southern France. Topography again seems to be playing a dominant role. The pattern over land corresponds to the orography of the region (recall Fig. 1). The heaviest rainfall is simulated along the important barrier of the Alps, and the sharp topographic gradient of the topography of the eastern slopes toward the Po Valley is associated with a comparable gradient in the precipitation, both observed (Fig. 5) and simulated (Fig. 11a). The model forecast surface flow (Fig. 12), rich in moisture due to a long fetch over the Mediterranean Sea (Fig. 13), is being forced over the terrain by the synoptic-scale processes in this case. Further, significant CAPE is present, but not over the area of major precipitation; instead it is mostly over the Mediterranean Sea (Fig. 14).

Over the sea, the two bands of precipitation in Fig. 11a are associated with the front as it passes over the western Mediterranean from west to east. Although we have no data to validate the precipitation predicted by the model over the sea, Fig. 15 seems to confirm the timing (Figs. 11a,b) and the shape of the precipitation bands (broad east of the Balearic Islands and narrow over Corsica and Sardinia). At 1000 UTC, a single broad cloud band with a north–south orientation and some convection can be seen just east of the Balearics (Fig. 15a); at 1800 UTC, this band is weakening as another, narrow band with clear evidence of deep convection is present over Corsica and Sardinia (Fig. 15b).

Of some significance in this case is that the model simulation (Fig. 16) and the actual observations (see DRRA98) indicate that most of the rainfall associated with this system over land fell as nonconvective precipitation. Deep convection did develop but apparently stayed mostly over the sea or very near the coast. The nonconvective nature of the precipitation is perhaps one explanation for the excellent simulation in this case. As with the previous case, a reasonably accurate forecast

Unauthenticated | Downloaded 08/02/21 05:51 AM UTC

(a)

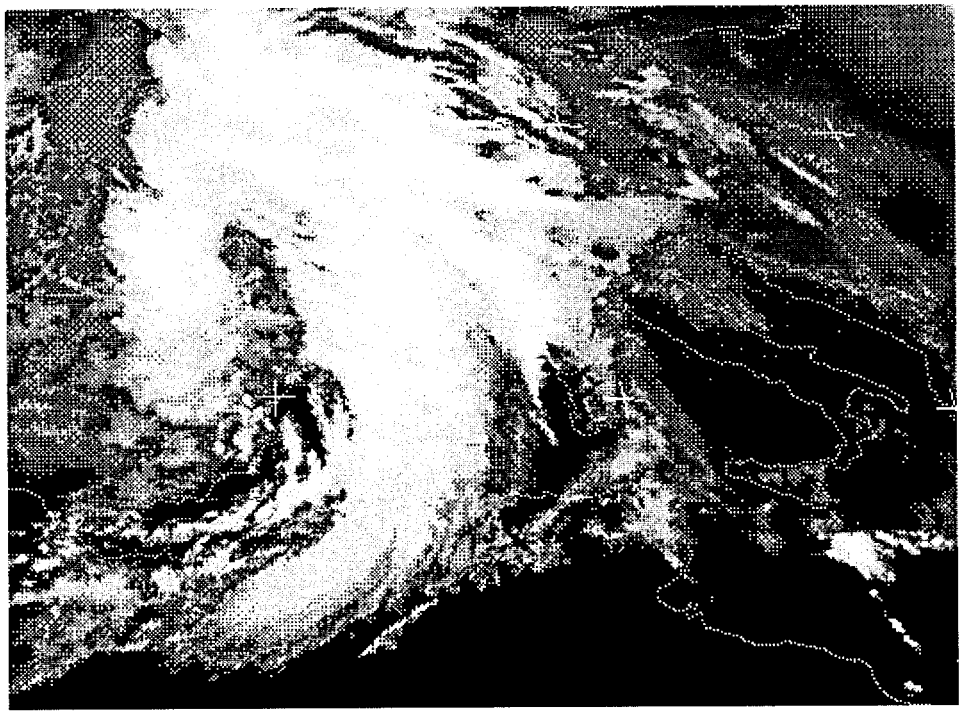

(b)

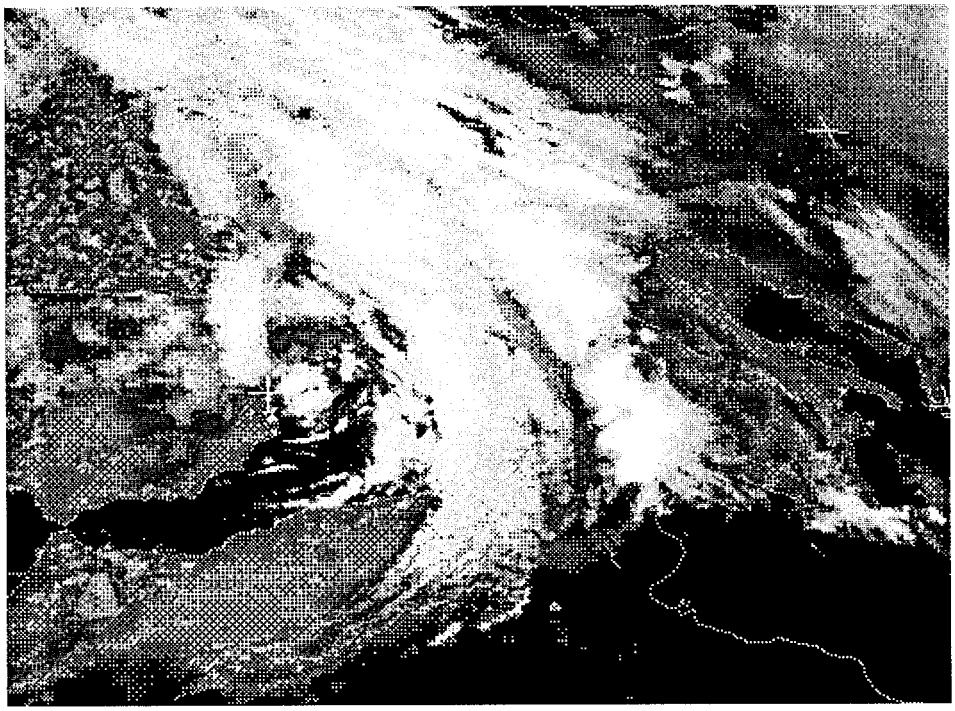

FIG. 15. Infrared Meteosat image for (a) 1000 UTC 5 November 1994 and 1800 UTC, (b) 5 November 1994.

Unauthenticated | Downloaded 08/02/21 05:51 AM UTC

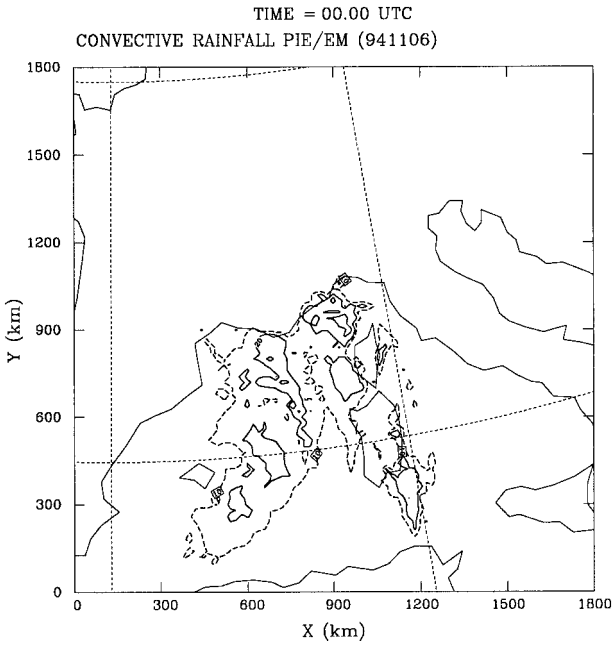


FIG. 16. As in Fig. 11a but for the convective part of the precipitation.

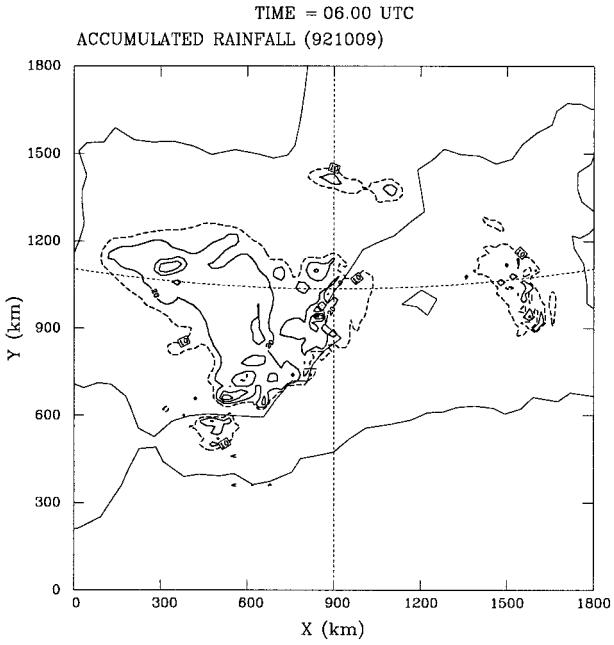


FIG. 17. Model forecast precipitation for the Menorca case, accumulated from 0600 UTC 8 October to 0600 UTC 9 October 1992. Contour interval is 20 mm starting at 20 mm (solid line); dashed countour corresponds to 10 mm.

of the low-level flow relative to the orography seems to yield good results.

### *c. Menorca*

Whereas the first two cases are dominated by the orographic influences interacting with the synoptic-scale systems, much of the important convection in this case occurred over the open seas of the western Mediterranean. As noted in Stensrud and Fritsch (1994), there can be cases wherein it is critical to have the details of the low-level tropospheric structure (notably, outflow boundaries) incorporated accurately in the initial conditions for the model. Given that the majority of the important events in this case occurred in the data-sparse oceanic areas of the western Mediterranean region, it can be anticipated that the model simulations in this case would be the least successful of the three. Not surprisingly, then, this is what the results reveal.

Although the model-predicted rainfall over mainland Spain is not too far from the observations (compare Figs. 7a and 17), over the sea the model fails to develop convection where it was observed to form. As noted in DRRA98, two convective systems began over the sea. One system remained nearly stationary for several hours and the other moved north-northeastward, eventually merging with the quasistationary system. After the merger, the combined system persisted and continued a north-northeastward movement, crossing the Balearic Islands (see Fig. 18 and the observed precipitation in Fig. 7b).

Whereas the model did not succeed in simulating these convective systems, it did seem to develop an environment favorable for supercell convection. That is, the model simulation showed the development of high values of CAPE and storm-relative environmental helicity (SREH) in the region where the convective systems developed. As discussed in DRRA98, there are reasons to believe that supercell storms were produced in this supercell-favorable [see Moller et al. (1994)] environment. The favorable environment, moreover, seemed to move along the western flanks of the observed storms (Fig. 19) and this evolution compares favorably with that derived from the ECMWF data (Figs. 19b and 20). This simulation suggests that the development of convection in the model depended on unobserved features that could not be included in the model initial conditions. It is encouraging, however, that the model seems to have done well in simulating the evolution of the convective *environment.*

## 5. Factor separation

Following Stein and Alpert (1993), we have attempted to isolate the effect of two factors by performing additional simulations (see Table 1). For the Algeria and Piedmont cases, we consider the impact of the orography and of the flux of water vapor from the Mediterranean Sea. These two factors have been chosen as likely candidates for consideration, based on the diagnostic work described in DRRA98. The Menorca case has not been considered since the results of the control run are not very promising (recall section

Unauthenticated | Downloaded 08/02/21 05:51 AM UTC

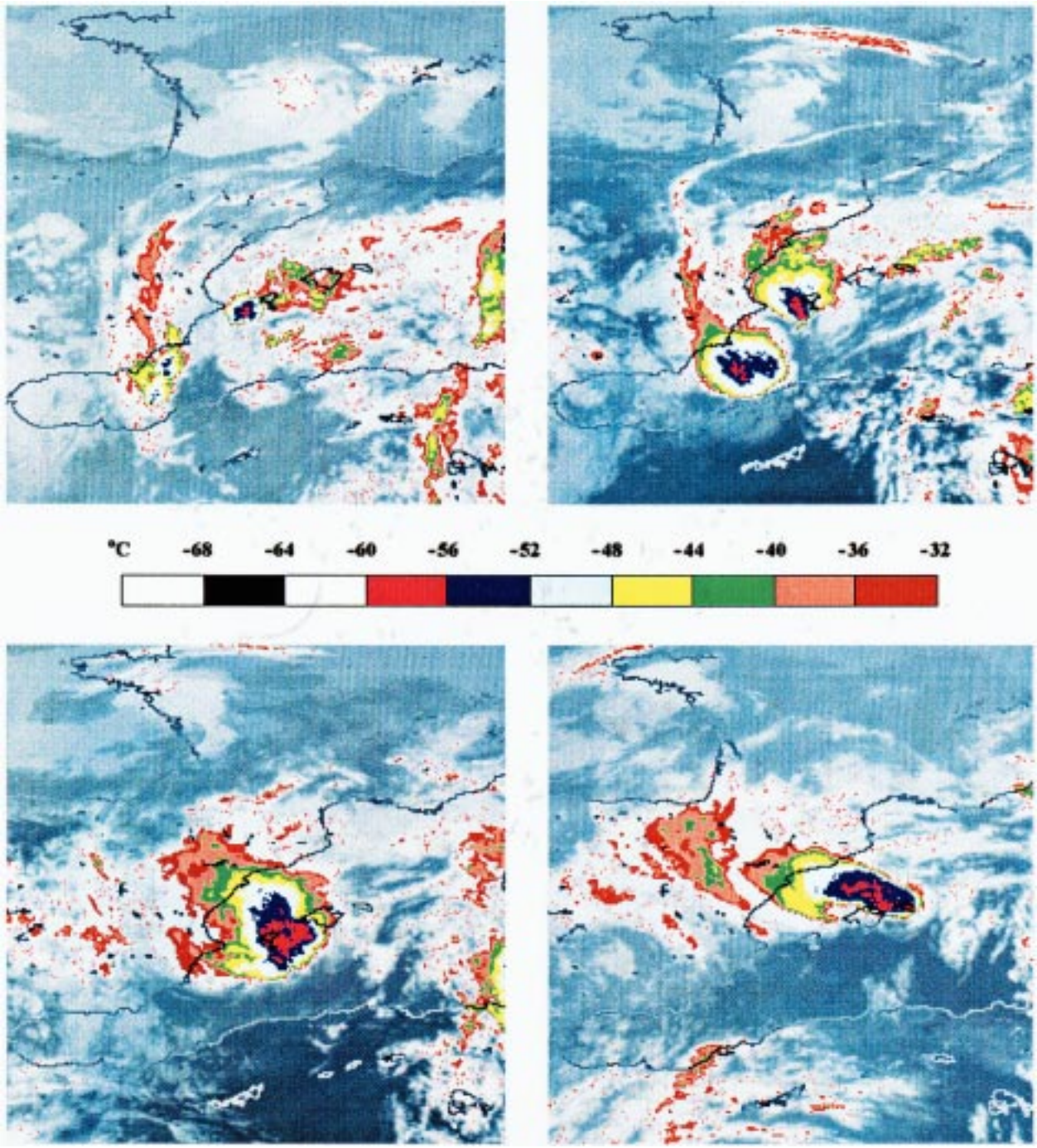


FIG. 18. Infrared Meteosat images on 8 October 1992 at (a) 0500 UTC, (b) 1000 UTC, (c) 1500 UTC, and (d) 2000 UTC.

4), and we have no way of validating quantitatively the model-simulated precipitation over the sea.

An important principle in factor separation is that when more than one factor is considered, it is not sufficient simply to compare a simulation done by removing some physical effect from the control simulation ($f_0$) with $f_0$. That is, there is a contribution associated with the interaction of two (or more) effects that must be considered. Generally, a complete factor separation for $n$ factors requires $2^n$ simulations, including the control run. For our purposes, with two factors under consideration, we need three additional simulations (Table 1) beyond the control run. The effect of orography is depicted by $f_2^* \equiv f_2 - f_1$; the effect of sea surface water vapor flux is shown by $f_3^* \equiv f_3 - f_1$; and the effect of the *interaction* between

Unauthenticated | Downloaded 08/02/21 05:51 AM UTC

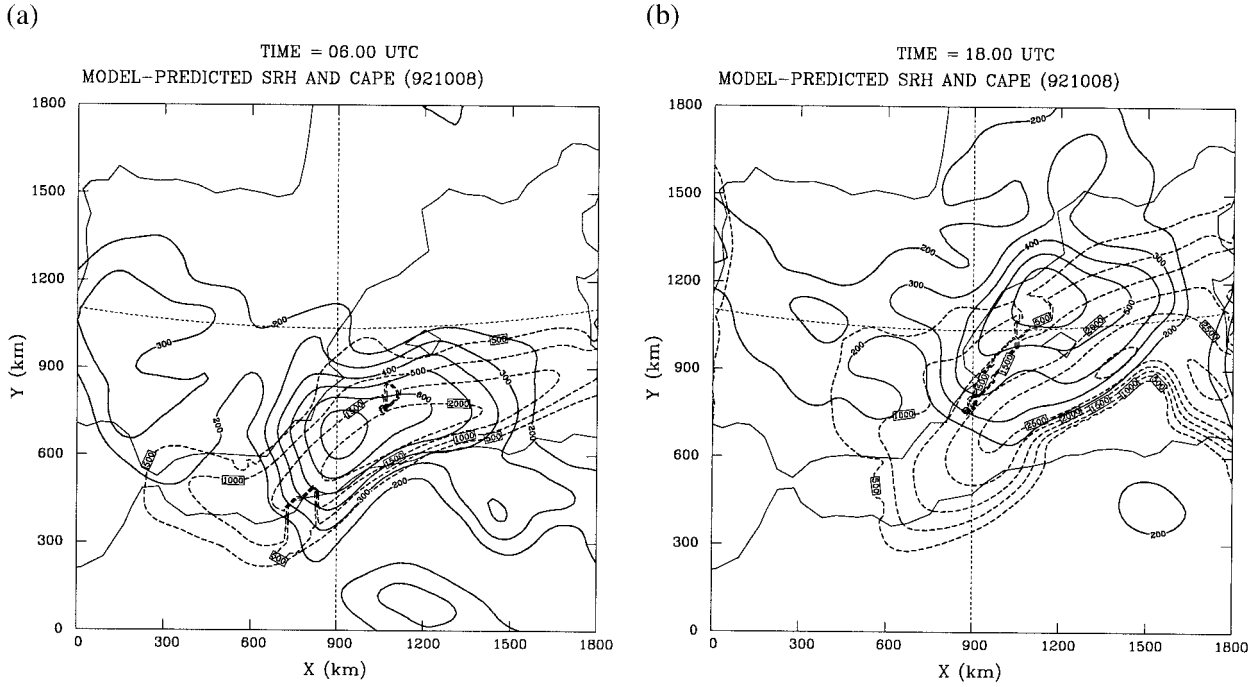


FIG. 19. Model forecast SREH (only positive values, solid line) and CAPE (dashed line) for the ''Menorca case'': (a) at 0600 UTC 8 October 1992 and (b) at 1800 UTC 8 October 1992. The estimated storm motion (from Fig. 18) is 17 m $s^{-1}$, from 220°. Contour interval for SREH is 100 $m^2$ $s^{-2}$, starting at 200 $m^2$ $s^{-2}$. Contour interval for CAPE is 500 J $kg^{-1}$, starting at 500 J $kg^{-1}$.

orography and sea surface water vapor flux is given by $f_{23}^* \equiv [f_0 - (f_2 + f_3)] + f_1$.

### *a. Algeria*

Simulation $f_1$ results in precipitation amounts of less than 10 mm nearly everywhere (Fig. 21). These amounts indicate that the synoptic forcing alone is not capable of producing significant precipitation for this event. The effect of orography on the precipitation and the low-level winds (from the $f_2^*$ simulation for this case; Figs. 22 and 23, respectively) indicate that the topography is a major factor in the precipitation, but the precipitation quantities are less than shown in the control run. Orography is very important in the simulation of the wind flow at low levels over the eastern Spanish coast. Near Gibralter, the orography channels the flow between the mountain ranges in southern Spain and northern Africa. A weak cyclonic circulation is depicted along the Algerian coast; thus, this ''Algerian low'' is confirmed to be due to orography and, as noted in DRRA98, this feature enhanced the easterly flow toward the Spanish coast during the heavy precipitation event.

Evaporation from the sea (simulation $f_3^*$, Fig. 24) is acting to increase the rainfall in a concentrated area over the eastern Spanish coast and over the sea. Since no orography is included in this experiment, the coastal effects are probably associated with the increased surface roughness in the model over the land. Changes to

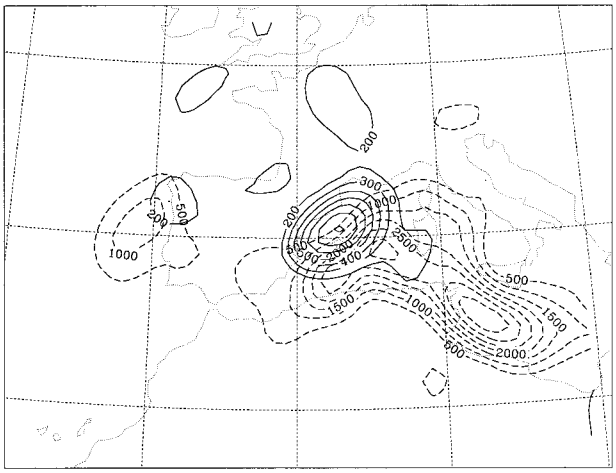

FIG. 20. As in Fig. 19b but with SREH and CAPE calculated using the ECMWF data.

TABLE 1. Simulations performed to support the factor separation for each case, and identification of the notation for the type of simulation ($f_i$, $i$ = 0, 1, 2, 3).

| | Experiment | Case | | |
|---|---|---|---|---|
| | | Algeria | Piedmont | Menorca |
| $f_0$ | Full physics (control run) | X | X | X |
| $f_1$ | No orography, no surface flux | X | X | |
| $f_2$ | Orography, no surface flux | X | X | |
| $f_3$ | No orography, surface flux | X | X | |

Unauthenticated | Downloaded 08/02/21 05:51 AM UTC

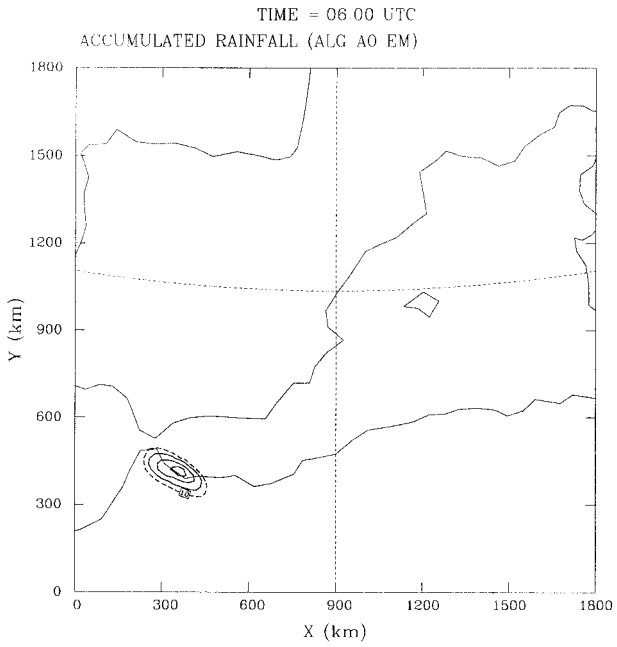


FIG. 21. Precipitation forecast valid at 0600 UTC 2 February 1993 (the end of the simulation) for simulation $f_1$, with no orography and no surface flux of water vapor from the sea; dashed contour is 10 mm, solid contour interval at 20 mm, starting at 20 mm.

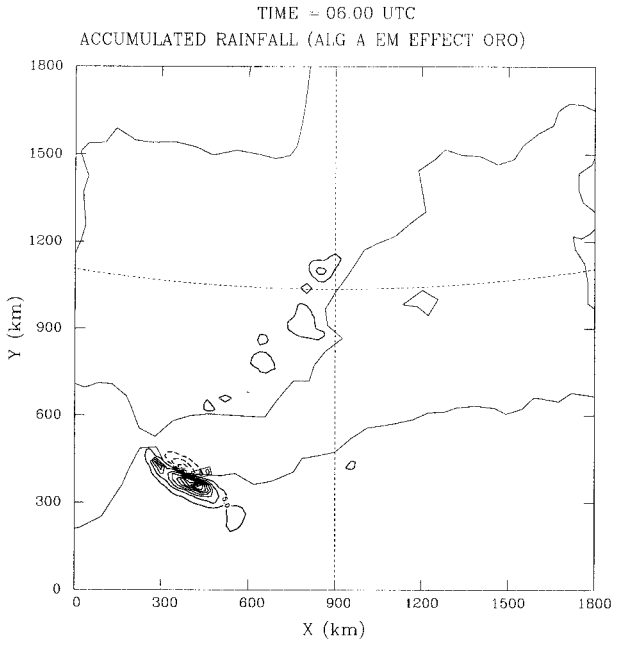


FIG. 22. Precipitation forecast valid at 0600 UTC 2 February 1993 (the end of the simulation) for simulation $f_2^*$, showing the effect of orography; dashed contours show a negative contribution, solid contours show a positive contribution. The contour interval is 10 mm, starting at $\pm 5$ mm.

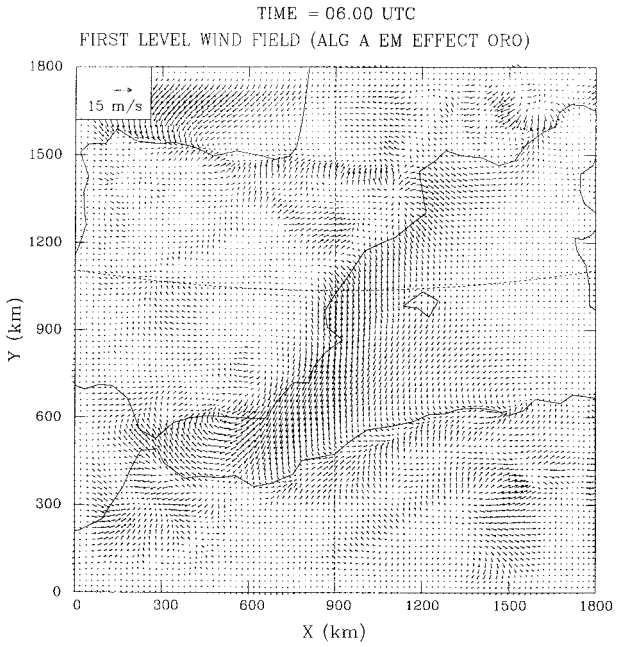


FIG. 23. Wind forecast at the lowest model level (4.5 m AGL) valid at 0600 UTC 2 February 1993 (the end of the simulation) for simulation $f_2^*$, showing the effect of orography; for comparison, a vector of 15 m $s^{-1}$ is shown in the upper-left corner.

the low-level flow attributable to evaporation from the sea (not shown) are negligible.

The interaction between orography and evaporation from the sea ($f_{23}^*$, Fig. 25) is the most important effect in the simulation. Its pattern accounts for most of the

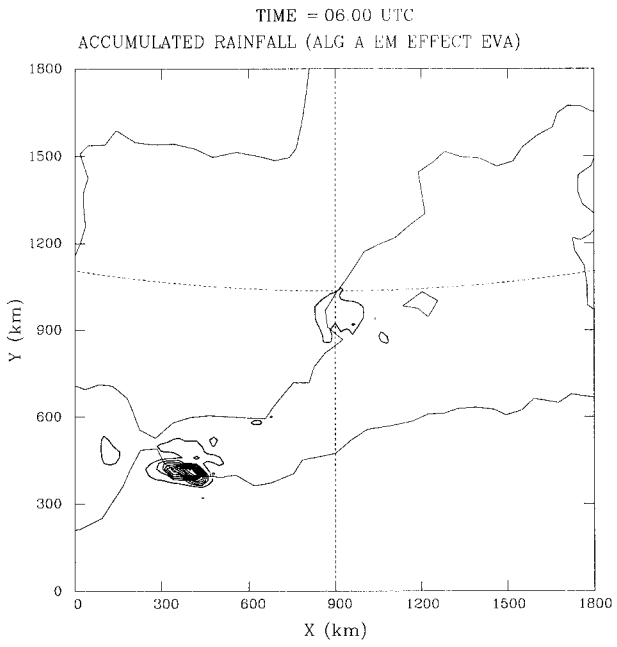


FIG. 24. As in Fig. 22 except for simulation $f_3^*$, showing the effect of evaporation from the sea.

Unauthenticated | Downloaded 08/02/21 05:51 AM UTC

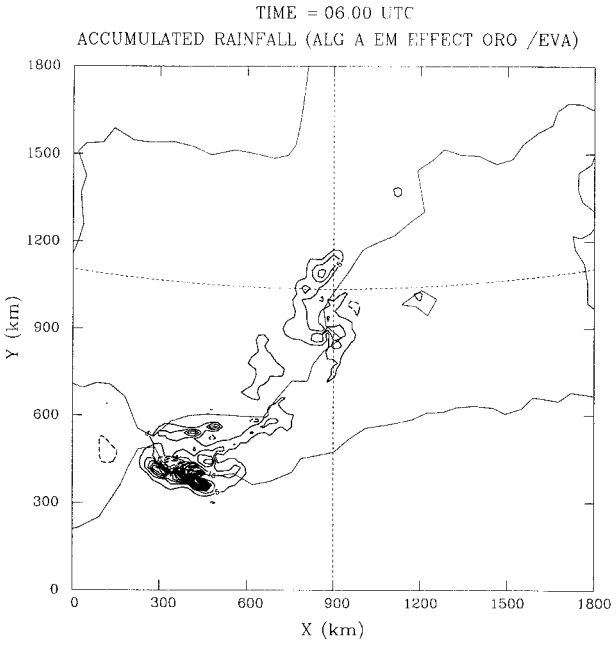


FIG. 25. As in Fig. 22 except for simulation $f_{23}^{*}$, showing the effect of the interaction between orography and evaporation from the sea.

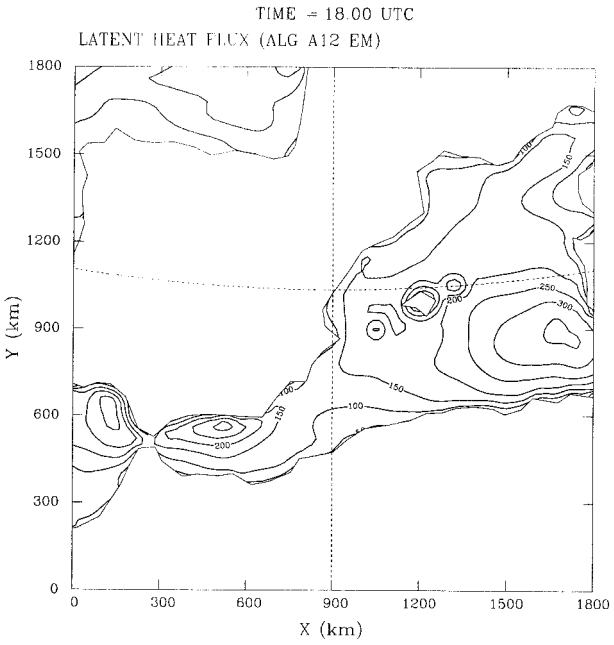


FIG. 26. Latent heat flux from the sea (contour interval of 50 W $m^{-2}$) at 1800 UTC 1 February 1993, halfway through the simulation.

model-simulated precipitation (compare Fig. 25 with Fig. 9a). As discussed in DRRA98 and demonstrated in Fig. 26, large water vapor flux from the Mediterranean Sea is carried toward the eastern Spanish coast by the low-level flow, where it interacts with the orography. The effect of the interaction is not very influential on the low-level winds, except in eastern Spain, where it is contributing to upslope flow (not shown).

### *b. Piedmont*

The observed precipitation (Fig. 5) and the mesoscale model's forecast of precipitation (Fig. 14a) certainly suggest an important role for orography in this event. As in Romero et al. (1997), it is possible to argue that evaporation from the Mediterranean was not important in this case. The moisture content of the air flowing northward toward the Alps, between the Italian peninsula and the islands of Corsica and Sardinia, is very high (see Fig. 13), while the evaporation in the same area is modest (Fig. 27). Thus, the atmosphere apparently already contains considerable moisture at low levels and any additional contribution from sea surfaces fluxes is not likely to be important in this case. Romero et al. (1997) have obtained similar results in another case.

Orographic effects on the low-level wind at the end of the simulation (Fig. 29) show two different aspects. First, the blocking action of the Alps on the windward side, stronger in the central part of the Alps than elsewhere, increases the wind along the Po Valley toward the Piedmont region. Further, there are strong downslope winds in the lee of the Alps. Second, the orographic influence on the front in the Mediterranean appears to be significant; in the $f_2$ experiment, the front is farther east than when orography is included, indicating that Corsica and Sardinia are acting to delay the passage of the front. The orographic influence on precipitation during the first half of the simulation (Fig. 28a) is most

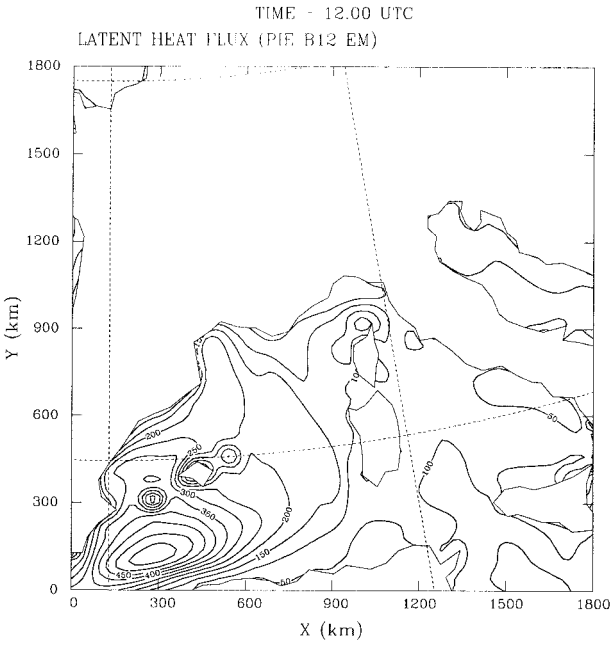


FIG. 27. As in Fig. 26 but for 1200 UTC 5 November 1994 (halfway through the simulation).

Unauthenticated | Downloaded 08/02/21 05:51 AM UTC

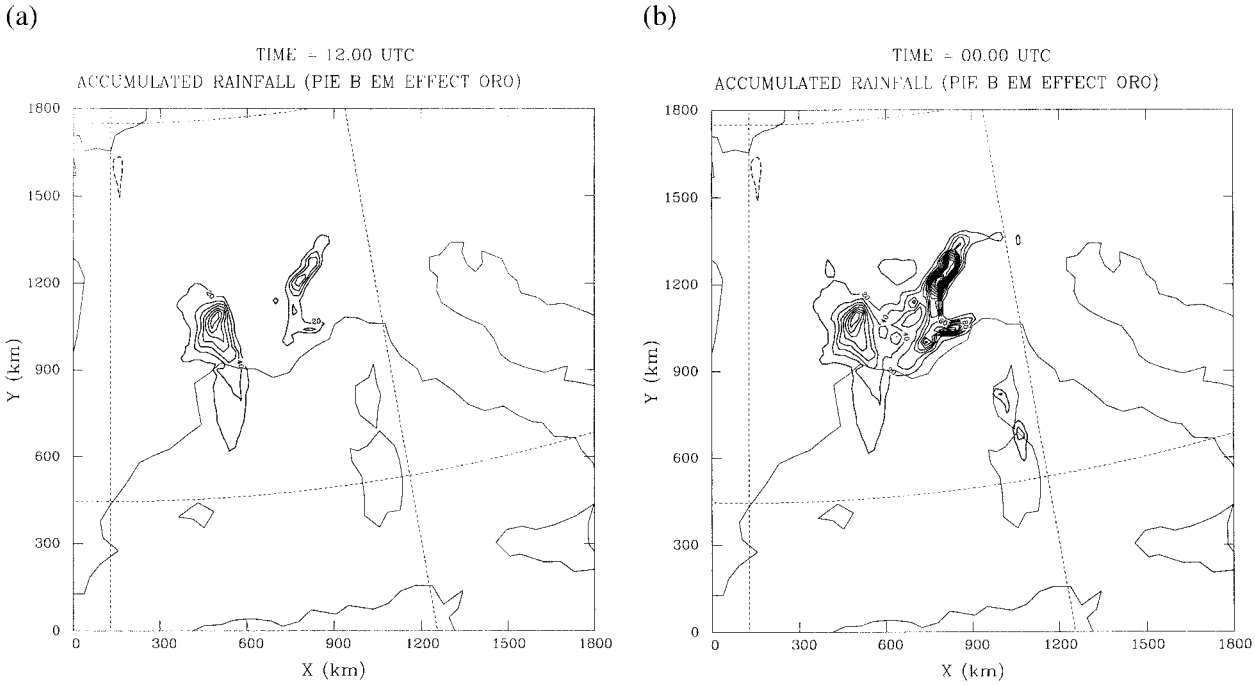


FIG. 28. Precipitation forecast valid at (a) 1200 UTC 5 November 1994 (halfway through the simulation) and (b) 0000 UTC 6 November (the end of the simulation) for simulation $f_2^*$, showing the effect of orography; dashed contours show a negative contribution, solid contours show a positive contribution. The contour interval is 20 mm, starting at ±20 mm.

apparent over the Central Massif (recall Fig. 1) in France, and over the Alps by the end of the simulation (Fig. 28b). The latter closely matches the precipitation pattern for the Piedmont event (compare with Fig. 5).

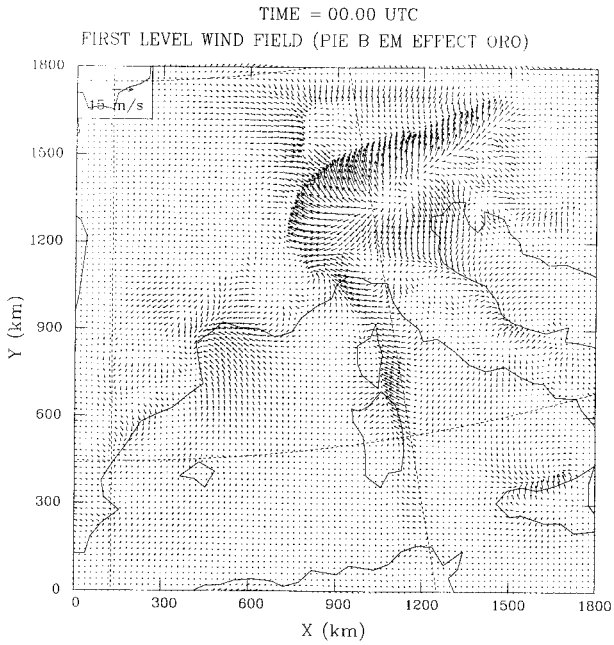


FIG. 29. As in Fig. 23 except for 0000 UTC 6 November 1994 (the end of the simulation).

The effect of evaporation from the sea on the low-level wind field (not shown) is weak. As anticipated, its impact on the precipitation is also weak (see Fig. 30); the effect is positive but is mostly restricted to the open sea between Corsica and Sardinia and the Balearic Islands. As shown in Fig. 31, the impact on the Piedmont region's precipitation is small through the end of the simulation. However, the interaction's importance is positive and substantial over the Central Massif in France. There are both positive and negative contributions to precipitation from the interaction over the western slopes of the Alps, albeit somewhat smaller than to the west (over the Central Massif), implying a complex redistribution of rainfall. Unlike the Algeria case, where the interaction was critical, the Piedmont case shows the interaction to be relevant primarily over France's Central Massif, not in the region where the event was most intense.

## 6. Discussion and forecasting implications

These results appear to validate our basic hypothesis, in terms of the feasibility of applying mesoscale forecast models to the task of operational forecasting in the western Mediterranean. That is, it appears that the combination of the synoptic-scale structures associated with the region's heavy rainfall events and the strong topographic influences combine to provide an opportunity for improved forecasting through the use of mesoscale model simulations. If operational forecasters had the

Unauthenticated | Downloaded 08/02/21 05:51 AM UTC

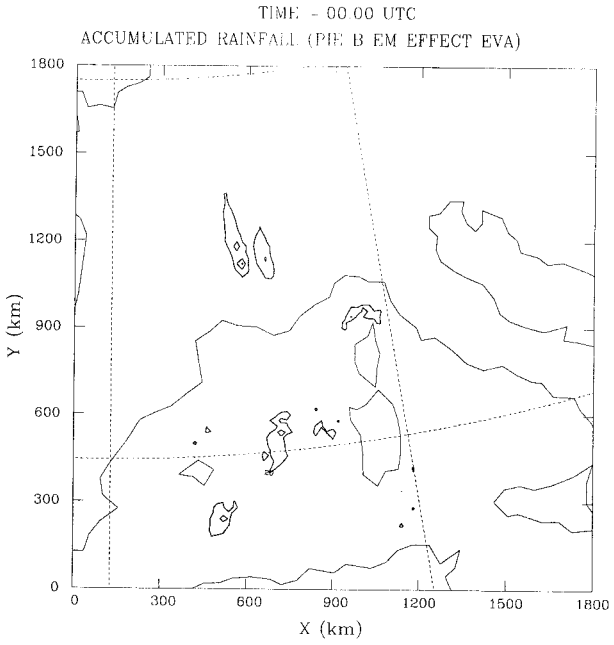


FIG. 30. Precipitation forecast valid at 0000 UTC 6 November 1994 (the end of the simulation) for simulation $f_2^*$, showing the effect of evaporation; dashed contours show a negative contribution, solid contours show a positive contribution. The contour interval is 20 mm, starting at $\pm 20$ mm.

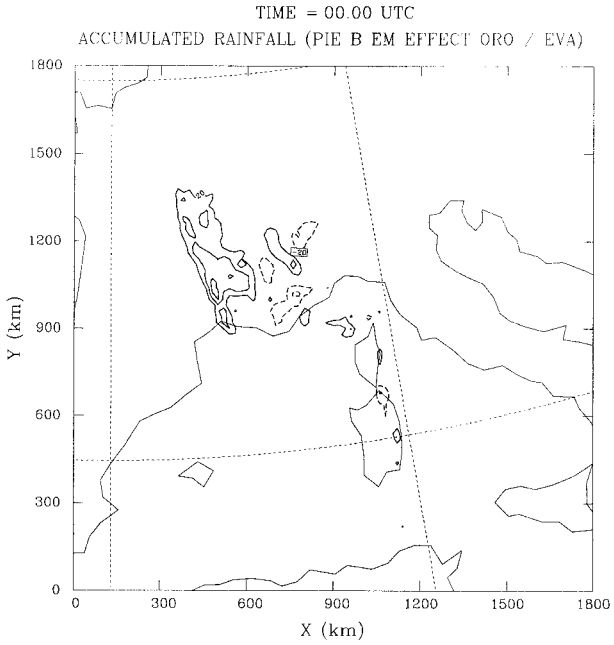


Fig. 31. As in Fig. 28 except for simulation $f_{23}^*$, showing the effect of the interaction between orography and evaporation from the sea.

model results of section 4 available to them in real time, we believe they would have found this to be useful information in making their forecasts. However, this study by itself does not constitute a *definitive* answer to the questions posed in section 1. That is, after only three case studies, we are not prepared to make an unqualified recommendation for the implementation of an operational mesoscale model in Spain. There are several issues yet to be addressed before it would be appropriate to make such a recommendation.

Clearly, it is necessary to validate more extensively the notion that most heavy rainfalls in the region share similar synoptic-scale structures. It is unrealistic to expect that all heavy precipitation events fit this pattern, but it would be valuable to have some quantitative idea of the frequency at which such events do arise in broadly similar synoptic-scale patterns. In order to make good use of mesoscale model guidance, then, a forecaster needs to know in what circumstances the model is likely to be successful and when it is likely to fail. For our three cases, the precipitation guidance was quite good for the first two cases, and inadequate for the third. However, the convective storm *environment* was apparently well simulated in the third; it is possible, although we have not demonstrated it, that the simulation only lacked mesoscale initial data to capture the development of the convection. Would an operational model produce similar results? If there was a way to introduce the mesoscale details artificially (e.g., by manual intervention during the initialization), would the model then produce useful precipitation guidance? These questions remain unanswered.

Our study began with the a priori knowledge that each case did, in fact, involve a heavy rainfall event. A forecaster does not have such knowledge, of course. This leads to another important unanswered question. How often would an operational mesoscale model be successful in recognizing situations where the synoptic pattern apparently fits that of a heavy rainfall event but the event does *not* happen? Another set of simulations is needed with events that are at least superficially similar to our heavy rainfall cases but wherein no significant rainfalls occur. Large-amplitude gravity waves, but with no precipitation, have been observed in the western Mediterranean region in similar synoptic patterns (Ramis and Jansá 1983; Monserrat et al. 1991). This problem (the forecast of a nonevent in an apparently threatening synoptic situation) can be very challenging to an operational forecaster [see Stensrud and Maddox (1988)].

The satellite images (Figs. 15, 18, and Fig. 13 of DRRA98) and the numerical simulations show that convection was present (if not always dominant) in all three of our cases. The importance of convection to the region's heavy precipitation meteorology is well known (García-Dana et al. 1982). Given the dominant role of deep moist convection, any implementation of a mesoscale model must include careful consideration of how to treat deep convection in the simulations. The parameterization used in this study [i.e., that of Emanuel (1991)] seems to have done reasonably well. Nevertheless, the successful representation of cumulus convec-

Unauthenticated | Downloaded 08/02/21 05:51 AM UTC

tion is far from being a closed book; the superiority of any convective parameterization or even the explicit calculation of convective processes depends on such issues as model resolution, the region of application, peculiarities associated with particular events, and computational expense. More simulations of cases using different methods for accounting for convection [e.g., Kain and Fritsch (1990)] are needed to evaluate which approach is most appropriate for the western Mediterranean region. The evaluation, moreover, should not be limited to the success of the precipitation prediction alone. Various low-level wind flows that are associated with the region's topography [see Bougeault et al. (1990)] are an important issue in the region's weather and a successful mesoscale model needs to provide guidance about those processes, as well.

In our cases, it appears that some simple diagnostic outputs can be a valuable supplement to precipitation forecasts. As shown clearly from our factor separation experiments, the evaluation of upslope flow and consideration of sea surface water vapor flux can be quite pertinent for the region. Diagnostics relevant to these factors are both easy to do and likely to be informative to forecasters. Convective storm environment parameters derived from the simulations, such as SREH, can be quite valuable in assessing the potential hazards from convection even when the model is not successful in simulating the convection itself, as our Menorca case suggests.

The QPF capability of the mesoscale model we used is certainly encouraging but the magnitudes of the simulated precipitation tend to be underestimates, especially with respect to the highly localized peak amounts in convective situations. In fact, it is these peak values that typically are responsible for many of the flash floods that produce significant damage and numerous casualties in the region (García-Dana et al. 1982). Obviously, the model resolution is at least partly responsible for this. However, we believe there is still reason to explore the possibility of improving this facet of mesoscale models; this research is already under way. Another promising line of research will pursue the use of high-resolution models in regions of complex orography. For example, the Gandía area in Valencia (the prominent cape in eastern Spain shown in Fig. 7a) exhibits a climatological maximum in precipitation during heavy rainfall events (Font 1983). In fact, this can be seen in our Figs. 3, 7a, and 10. This area is characterized by a basin-shaped terrain configuration, which might explain the localized nature of the extreme precipitation observed there repeatedly.

We believe there is cause for guarded optimism about the use of mesoscale models to improve operational forecasts of heavy rainfall in the region. With continued testing of these concepts, if our early results prove to be representative, an implementation of this concept for operations should be a relatively simple task.

*Acknowledgments.* This work was partially supported by EC under Grant EV5V-CT94-0442. Charles Doswell was visiting the University of the Balearic Islands (UIB) during the inception of the research under Grant DGICYT SAB95-0136. Mr. Danny V. Mitchell was very helpful during the model development and testing carried out during C. Doswell's visit to UIB.

## REFERENCES

Arakawa, A., and W. H. Schubert, 1974: Interaction of a cumulus cloud ensemble with the large-scale environment, Part I. *J. Atmos. Sci.,* **31,** 674–701.

Benjamin, S. G., and T. N. Carlson, 1984: Some effects of surface heating and topography on the regional severe storm environment. Part I: Three-dimensional simulations. *Mon. Wea. Rev.,* **114,** 307–329.

Bhumralkar, C. M., 1975: Numerical experiments on the computation of ground surface temperature in an atmospheric general circulation model *J. Appl. Meteor.,* **14,** 1246–1258.

Blackadar, A. K., 1976: Modeling the nocturnal boundary layer. *Proc. Third Symp. Atmospheric Turbulence, Diffusion and Air Quality,* Raleigh, NC, Amer. Meteor. Soc., 46–49.

Bougeault, P., and P. Lacarrère, 1989: Parameterization of orography-induced turbulence in a mesobeta-scale model. *Mon. Wea. Rev.,* **117,** 1872–1890.

——, A. Jansá, B. Benech, B. Carissimo, J. Pelon, and E. Richard, 1990: Momentum budget over the Pyrenees: The PYREX experiment. *Bull. Amer. Meteor. Soc.,* **71,** 806–818.

Davies, H. C., 1976: A lateral boundary formulation for multilevel prediction models. *Quart. J. Roy. Meteor. Soc.,* **102,** 405–418.

Davies-Jones, R. D., D. Burgess, and M. Foster, 1976: Test of helicity as a tornado forecast parameter. Preprints, *16th Conf. Severe Local Storms,* Kananaskis Park, AB, Canada, Amer. Meteor. Soc., 588–592.

Doswell, C. A., III, C. Ramis, R. Romero, and S. Alonso, 1998: A diagnostic study of three heavy precipitation episodes in the western Mediterranean region. *Wea. Forecasting,* **13,** 102–124.

Emanuel, K. A., 1991: A scheme for representing cumulus convection in large-scale models. *J. Atmos. Sci.,* **48,** 2313–2335.

Fernández, C., M. A. Gaertner, C. Gallardo, and M. Castro, 1995: Simulation of a long-lived meso-$\beta$ scale convective system over the Mediterranean coast of Spain. Part I: Numerical predictability. *Meteor. Atmos. Phys.,* **56,** 157–179.

Font, I., 1983: Climatology of Spain and Portugal (in Spanish). Instituto Nacional de Meteorología, 296 pp. [Available from Instituto Nacional de Meteorologia, Apartado 285, 28071 Madrid, Spain.]

Fritsch, J. M., and C. F. Chappell, 1980: Numerical prediction of convectively driven mesoscale pressure systems. Part I: Convective parameterization. *J. Atmos. Sci.,* **37,** 1722–1733.

García-Dana, F., R. Font, and A. Rivera, 1982: Meteorological situation during the heavy rain event in the eastern zone of Spain during October 82 (in Spanish). Instituto Nacional de Meteorología, 80 pp. [Available from Instituto Nacional de Meteorología, Apartado 285, 28071 Madrid, Spain.]

Kain, J. S., and J. M. Fritsch, 1990: A one-dimensional entraining/detraining plume model and its application in convective parameterization. *J. Atmos. Sci.,* **47,** 2784–2802.

Llasat, M. C., 1987: Heavy rain events in Catalonia: Genesis, evolution and mechanism (in Spanish). Ph.D. thesis, University of Barcelona, Barcelona, Spain, 543 pp. [Available from Dept. de Publicacions, Universitat de Barcelona, Auda. Diadonal 647, 08028 Barcelona, Spain.]

Louis, J. F., 1979: A parametric model of vertical eddy fluxes in the atmosphere. *Bound.-Layer Meteor.,* **17,** 187–202.

Mahfouf, J. F., E. Richard, and P. Mascart, 1987a: The influence of

Unauthenticated | Downloaded 08/02/21 05:51 AM UTC

soil and vegetation on the development of mesoscale circulations. *J. Climate Appl. Meteor.,* **26,** 1483–1495.

——, ——, ——, E. C. Nickerson, and R. Rosset, 1987b: A comparative study of various parameterizations of the planetary boundary layer in a numerical mesoscale model. *J. Climate Appl. Meteor.*, **26,** 1671–1695.

Mahrer, Y., and R. A. Pielke, 1977: The effects of topography on the sea and land breezes in a two-dimensional numerical model. *Mon. Wea. Rev.,* **105,** 1151–1162.

Meteorological Office, 1954: *Weather in the Mediterranean.* Air Ministry, 362 pp.

Moller, A. R., M. P. Foster, C. A. Doswell III, and G. R. Woodall, 1994: A supercell thunderstorm spectrum and its application in the operational environment. *Wea. Forecasting,* **89,** 327–347.

Monserrat, S., C. Ramis, and J. A. Thorpe, 1991: Large amplitude pressure oscillations in the western Mediterranean. *Geophys. Res. Lett.,* **18,** 183–186.

Nickerson, E. C., E. Richard, R. Rosset, and D. R. Smith, 1986: The numerical simulation of clouds, rain and airflow over the Vosges and Black Forest mountain: A meso-$\beta$ model with parameterized microphysics. *Mon. Wea. Rev.,* **114,** 398–414.

Paccanella, T., S. Tibaldi, R. Buizza, and S. Scoccianti, 1992: High-resolution numerical modeling of convective precipitation over northern Italy. *Meteor. Atmos. Phys.,* **50,** 143–163.

Pedder, M. A., 1989: Limited area kinematic analysis by a multivariate statistical interpolation method. *Mon. Wea. Rev.,* **117,** 1695–1708.

——, 1993: Interpolation and filtering of spatial observations using successive corrections and Gaussian filters. *Mon. Wea. Rev.,* **121,** 2889–2902.

Pinty, J. P., 1984: Une méthode variationnelle d'ajustement des champs de masse et de vent. Note 72 de l'I.O.P.G., Université de Clermont II, 20 pp. [Available from Observatoire de Physique du Globe de Clermont-Ferrand, 12 Ave. des Landais, F-63000 Clermont-Ferrand, France.]

——, P. Mascart, E. Richard, and R. Rosset, 1989: An investigation of mesoscale flows induced by vegetation inhomogeneities using an evapotranspiration model calibrated against HAPEX-MOBILHY data. *J. Appl. Meteor.,* **28,** 976–992.

Ramis, C., and A. Jansá, 1983: Meteorological conditions simultaneous to large sea level oscillations in the western Mediterranean (in Spanish). *Rev. Geofis.,* **39,** 35–42.

——, and R. Romero, 1995: A first numerical simulation of the development and structure of the sea breeze in the island of Mallorca. *Ann. Geophys.,* **13,** 981–994.

——, A. Jansá, S. Alonso, and M. A. Heredia, 1986: Convection over the western Mediterranean. Synoptic study and remote observation (in Spanish). *Rev. Meteor.,* **7,** 59–82.

——, M. C. Llasat, A. Genovés, and A. Jansá, 1994: The October 1987 floods in Catalonia: Synoptic and mesoscale mechanisms. *Meteor. Applicat.,* **1,** 337–350.

Raymond, D. J., and A. M. Blyth, 1986: A stochastic model for nonprecipitating cumulus clouds. *J. Atmos. Sci.,* **43,** 2708–2718.

Richard, E., P. Mascart, and E. C. Nickerson, 1989: The role of surface friction in downslope windstorms. *J. Appl. Meteor.,* **28,** 241–251.

Romero, R., S. Alonso, E. C. Nickerson, and C. Ramis, 1995: Influence of vegetation on the development and structure of mountain waves. *J. Appl. Meteor.,* **34,** 2230–2242.

——, C. Ramis, and S. Alonso, 1997: Numerical simulation of an extreme rainfall event in Catalonia: Role of orography and evaporation from the sea. *Quart. J. Roy. Meteor. Soc.,* **123,** 537–559.

Shapiro, R., 1970: Smoothing, filtering and boundary effects. *Rev. Geophys. Space Phys.,* **8,** 359–387.

Stein, V., and P. Alpert, 1993: Factor separation in numerical simulations. *J. Atmos. Sci.,* **50,** 2107–2115.

Stensrud, D. J., and R. A. Maddox, 1988: Opposing mesoscale circulations: A case study. *Wea. Forecasting,* **3,** 189–204

——, and J. M. Fritsch, 1994: Mesoscale convective systems in weakly forced large-scale environments. Part III: Numerical simulations and implications for operational forecasting. *Mon. Wea. Rev.,* **122,** 2084–2104.

Therry, G., and P. Lacarrère, 1983: Improving the eddy-kinetic energy model for planetary boundary layer description. *Bound.-Layer Meteor.,* **25,** 63–88.

Warner, T. T., R. A. Anthes, and A. L. McNab, 1978: Numerical simulations with a three-dimensional mesoscale model. *Mon. Wea. Rev.,* **106,** 1079–1099.

Unauthenticated | Downloaded 08/02/21 05:51 AM UTC